Development of A Micro-Scale Impact Tester for Characterizing Dynamic Properties of Biological Structural Materials

Nicklas Roth

Thesis submitted to the faculty of the Virginia Polytechnic Institute and State University in partial fulfillment of the requirements for the degree of

Master of Science
in
Mechanical Engineering

Ling Li
Robert L. West
Francesco De Carlo

May 8, 2023
Blacksburg, Virginia

Keywords: projectile impact, micro-impact, materials, biological, bio-inspired, dynamic loading

Development of A Micro-Scale Impact Tester for Characterizing Dynamic Properties of Biological Structural Materials

Nicklas Roth

Abstract

This thesis presents the design and construction of a micro-scale, air powered, impact testing device for use in Virginia Tech's Biological and Bio-inspired Materials Laboratory. A brief overview of current projectile impact testers is presented along with motivation for the fabrication of a new testing system capable of firing a projectile with a maximum diameter of 0.5 mm at velocities ranging from 20 to 50 m/s. Initial design calculations and analysis were performed to optimize barrel length, projectile size, and air pressure for desired velocity ranges. Computer aided design was then utilized to create a digital model of the entire system before production began on the device.

Within the scope of this project was the development of a large-scale projectile impact tester as a proof of concept of the system's design that would later be utilized by other researchers as well as the micro-scale tester which carried over the lessons learned and design improvements from the larger device. The culmination of the project was the testing of biological samples (sea urchin spine cross sections) to prove the viability of the device and highlight its research niche. Future use cases and design improvements of the small-scale impact tester were also investigated as part of this thesis work.

Development of A Micro-Scale Impact Tester for Characterizing Dynamic Properties of Biological Structural Materials

Nicklas Roth

General Audience Abstract

This thesis encompasses the design and fabrication of both a large-scale projectile impact tester as a proof of concept design as well as a micro-scale version that carries over many of the design elements of the large version but is designed to fire projectiles for small scale biological material tests. Also included as part of this thesis is a breakdown of the various impact testers currently available within research to show why this project was necessary.

The project culminated in simple impact studies of sea urchin spines to showcase the capabilities of the impact tester in its current form as well as to outline some of the expanded properties that could be determined with simple experimental setup changes. From this impact study, it was determined that sea urchin spines are a leading candidate in the formulation of bio-inspired impact resistant ceramic foams as they have excellent energy absorption properties during dynamic loading. The calcite foam structure of the sea urchin spines proved to have better impact absorption capabilities in comparison to many current engineering materials used for impact resistance. The final part of this thesis is a brief overview of the planned future use cases of the device.

Acknowledgements

I will forever be grateful to Professor Li for allowing me to join his team as a young mechanical engineering undergraduate student with little background in biological materials but a will to learn. Through his tutelage, I was able to broaden my perspective on materials research and engineering in general, eventually becoming a graduate student in his lab. My time as a graduate student at the Biological and Bio-Inspired Materials lab was an incredible leaning opportunity, mainly due to the welcoming and intellectually fostering environment created by Dr. Li.

I would also like to thank my other two committee members, Professor West and Dr. De Carlo. I have taken almost every mechanical engineering design course that Professor West offers here at Virginia Tech and it is his passion and drive that has inspired me to hopefully focus in mechanical design engineering for the foreseeable future. Dr. De Carlo has been a steadfast supporter of my thesis work in Professor Li's lab and it was his guidance that helped me to solve the electronics aspect of my research.

Without the support of my fellow graduate students in the lab and their willingness to always talk through a problem and offer solutions, this thesis would never have reached its conclusion. I must thank Dr. Zhifei Deng and Shabaz Khan for collaborating with me on parts of this project and for spending the time to discuss needed features and improvements for the impact testers of this thesis. I also have to thank Chenhao Hu and Luini Chen for donating a day of their time to teach me how to create volumetric reconstructions. Without them I would have been completely lost in the endeavor. To the rest of the students in the Biological Materials Lab, Ravi Bollineni, Hongshun Chan, Yiming Tan, Yang Geng, and Edward Lee, thank you for the many discussions we shared over the years and for the inspiration both in and outside of research.

Finally, I would like to thank my parents and family. They have always stood by my side and encouraged me to follow my dreams wherever they may lead. Without their steadfast support, I would not be where I am today.

Contents

List of Figures

List of Tables

Chapter 1

Introduction

This thesis describes the development of a micro-scale projectile impact testing device to be utilized for experiments where a small projectile with relatively low velocity is needed to explore the impact properties and fracture mechanics of differing materials. A final velocity range of 20-50 m/s is the design goal of the tester with a maximum projectile diameter of 0.5 mm. The design must be configurable for use in different experimental setups such as a wide variation in target sample sizes as well as in conjunction with synchrotron-based ultrafast X-ray imaging and tomography measurement. The tester must also have a velocity range of 20-50 m/s to accommodate various impact loading conditions.

1.1 Background

To gain full understanding of a material's properties and behaviors, that material needs to be tested over a varying range of conditions. For engineering purposes, materials need to be examined for properties that are expected during practical use such as deformation state and amplitude, cycle, strain rate, fatigue, and life expectancy [1]. Traditionally, a material's quasi-static properties under all forms of loading conditions cannot be established through one type of test but rather has to be studied under a limited range of conditions and then extrapolated to fulfill the unknown ranges using similarity laws and dimensional analysis [2, 3]. However, this extrapolation starts to break down during high-speed deformation due to unexpected material behaviors at increasing strain rates and smaller size scales [1]. Increasingly, the need for a dynamic tester has emerged to accurately study material properties and fracture mechanics during dynamic loading conditions on a small-scale [4].

There are various types of impact methods and testers to characterize a materials response to dynamic loading with the premier being the pendulum-based impact tests, drop-weight impactors, Taylor impact tests, as well as ballistic and plate impact tests; listed in order of increasing impactor velocity and characteristic strain rate [1, 5]. The review in this chapter focuses on projectile impact testing due to the wide range of achievable impact velocities, projectile masses, and impactor shapes. **Figure 1** represents various impact testing methods with their various impact velocities against their relative projectile size. Also included are dashed lines representing constant characteristic strain along with several applications of the impact testing methods shown in italics [1]. This graph allows for the comparison of the different type of impact testers available in research and the specific velocities that they are designed to achieve with their respective projectile diameters (**Table 1**).

There is currently a gap between free-fall impact weights and projectile gun impact testers at the semi-micro to macro range which this thesis seeks to fill. This research gap needed to be filled in order to study biological samples which are often small and irregular in shape. The sample's characteristics necessitate a small projectile that does not have an extremely high velocity.

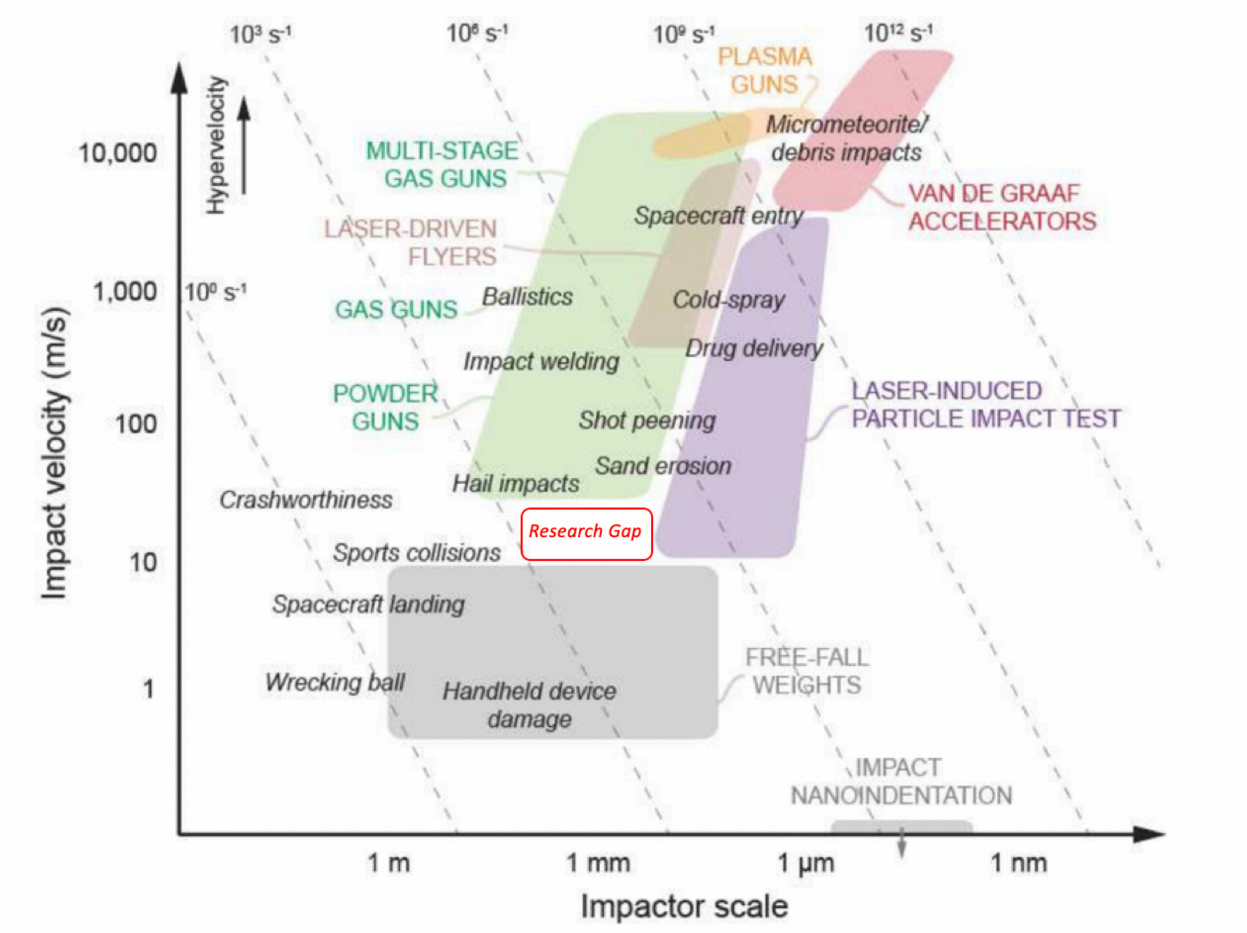

Figure 1: Various impact testing methods and several applications shown in uppercase and italic respectively. Dashed lines represent constant strain rates. The red gap represents the current lack of impact testing velocity and size range. Adapted from [1]

Table 1: Impact testing techniques with typical velocity ranges and projectile diameter. Adapted from [1]

Impact Methods	**Velocity Range**	**Projectile Dia. Range**
Free-Fall Weights	*0.8 - 10 m/s*	*50 µm - 1 m*
Powder Guns	*50 - 200 m/s*	*10 - 700 mm*
Gas Guns	*200 m/s - 2 km/s*	*0.5 - 10 mm*
Multi-Stage Gas Guns	*2 - 11 km/s*	*5 µm - 5 mm*
Laser Induced Particle Impactors	*10 m/s - 2 km/s*	*1 µm - 0.9 mm*
Laser Driven Flyers	*900 m/s - 8 km/s*	*20 µm - 1 mm*

1.2 Current Impact Testers in Research

Before discussing the motivation of this thesis project and its design, it is important to break down the different projectile impact testers. There are six main types of impactors widely used in research of small-scale impact events with those being single, double and triple stage gas guns, along with sabot-less drag acceleration systems, laser launched flyer plates, and laser induced particle impactors. The breakdown of these systems has been arranged in relative decreasing projectile size and increasing projectile speed. This is not a definitive ranking as the specifics of each device, such as velocity and impactor size, can be tailored to each experimental need which may blur the lines of the traditional classification [1].

1.2.1 Single Stage Gas Gun

The single stage gas gun is the simplest of systems for projectile research systems [6]. The design of this tester is outlined in **Figure 2**. It consists of a gas reservoir that is connected to a barrel by a valve and in some cases a breach for easy loading of a projectile. The term gas gun comes from the fact that a compressed gas is used to act as a propellant [1]. The compressed gas in the reservoir is released when a signal is sent to the solenoid valve. This accelerates the projectile along the barrel and into the sample located in the target box.

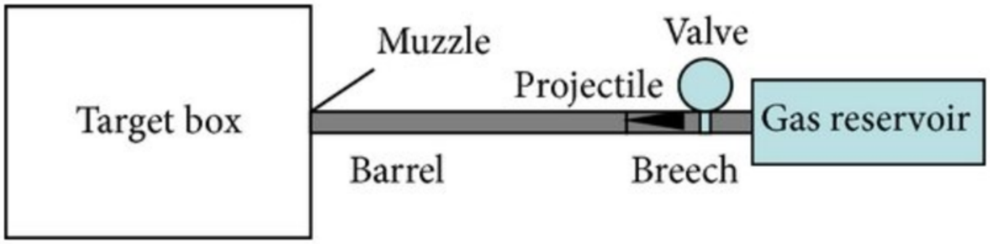

Figure 2: Gas gun setup for direct acceleration of a projectile, typically referred to as a single-stage gas gun. Adapted from [6]

1.2.2 Two-Stage Gas Gun

The two-stage gas gun is comparable to the single-stage gas gun however it utilizes a sabot to accelerate a projectile or particles towards a target and a respective catcher plate to separate the sabot from the chosen projectile. A sabot is some type of cup or container that the projectile(s) is placed in before being loaded into the barrel of the device. This ensures full energy transfer between the expanding gas from the reservoir while allowing for a varying size and number of projectiles instead of the traditional projectile that is determined by the barrel diameter of the device [7]. **Figure 3** details the end of barrel design required for a two stage gas gun with **Figure 3,i** showing the connected sabot and particles before catcher plate collision and the subsequent separation of the two with only the particles flying on towards the target (**Figure 3,ii**). A major proponent of this design is that it allows for firing of multiple particles towards a target at one time as well as a single projectile depending on size of the projectiles. This ‘shot-gun’ approach is used to increase the chances of a particle collision when utilizing small impactors and small targets however it does decrease the impact precision and control, relying more on chance to determine where a particle will hit [8, 9].

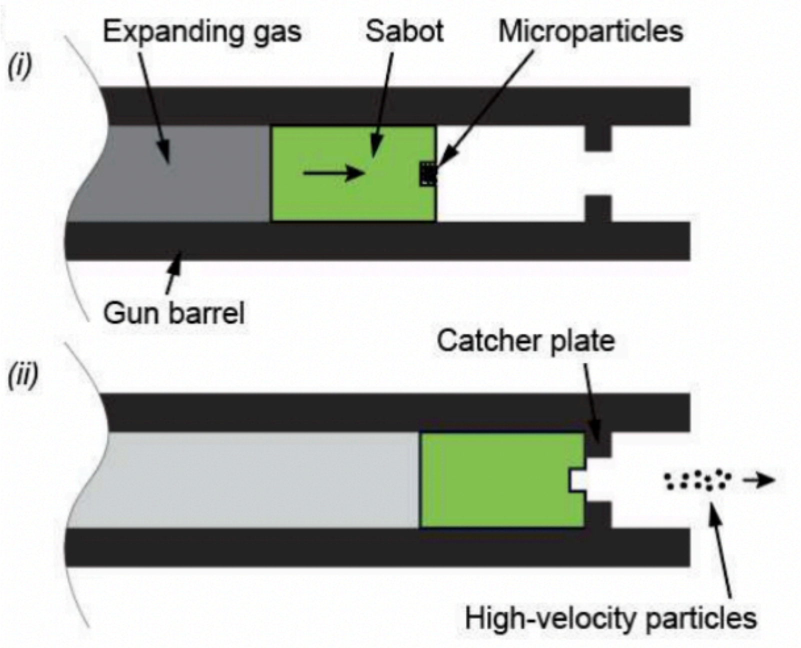

Figure 3: Setup for two stage LGG used primarily for millimeter to micrometer-sized particles. (i) Sabot and particles before catcher plate impact. (ii) Particle motion after sabot impact with catcher plate. Adapted from [1]

1.2.3 Three-Stage Gas Gun

The three-stage gas gun expands even further on the design of the gas gun system by adding in a graded-density impactor between the sabot and then end of the barrel along with a stationary buffer (**Figure 4**). This design relies on the momentum transfer from the moving sabot and graded impactor against the stationary buffer. The shock propagation through the buffer to the back surface of the holder leads to the detachment and acceleration of the stationary particles [1]. A graded-density impactor is utilized to tailor the drive conditions imparted onto the particles during the test, meaning that particle velocity distribution is highly consistent and the impact precision is greatly increased compared to that of a two-stage gas gun [10, 11]. A graded-density impactor is a metallic disk that is constructed of precisely oriented layers to generate the specific energy required for each impact velocity [11]. It is important to note that in sabot-based projectile impact testers the particle velocity is not determined by the particle mass but instead by the sabot mass and acceleration characteristics [1]. This effect is true as long as the particle mass is negligible compared to that of the sabot and results in the particles retaining the sabot velocity after separation [12]. For three-stage gas guns devices, the particle velocity relies on the particle's mass since the system relies on a momentum transfer between the particles at rest and the coupled sabot/graded-density impactor, making it a mass-dependent energy transfer. The energy transfer abides by the conservation of linear momentum equation and this is what allows for the greater velocities obtained by the three-stage impactor. There is an enormous mass difference between the moving sabot and stationary particles so for momentum to be conserved after impact the particle velocity must be exponentially higher than that of the sabot [11].

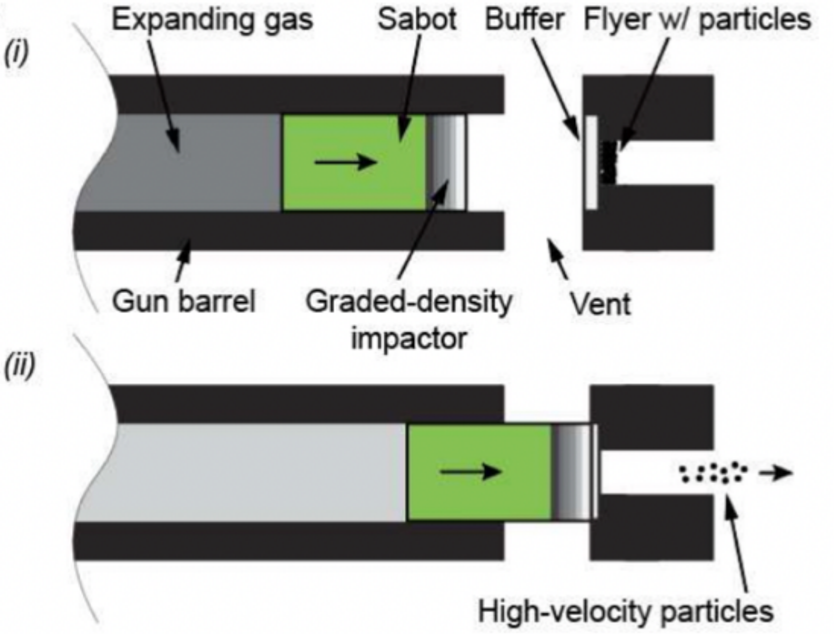

Figure 4: Three stage light gas gun. (i) Sabot and graded density impactor before collision with buffer and particles. (ii) Particle motion after impactor collision with buffer. Adapted from [1]

1.2.4 Sabot-Less Drag Acceleration System

The next type of particle impactor strays away from the definition of a gas gun but still uses a compressed gas or fluid flow to accelerate the projectile towards a target, known as sabot-less drag acceleration system. This system derives its name from the fact that the projectile is accelerated by its drag effect when introduced to a moving stream of gas [1]. Currently, there are two main types of drag acceleration systems, one in which a burst diaphragm is used with particles arranged on the surface of the diaphragm (**Figure 5**) and another which dispenses the projectile particles into a free-flowing gas (**Figure 6**) [1]. The first of these devices utilize a diaphragm, otherwise known as a burst disk, which is calibrated to rupture when a specific gas pressured is placed upon it. In a drag acceleration setup, these diaphragms are placed at the start of a barrel with the intended projectile particles oriented on the surface of the diaphragm. Once the pressure is sufficient to burst the diaphragm the particles are introduced to the compressed gas which in turn flows towards the target sample [13]. An important aspect of this system is that the method of particle delivery into the compressed gas allows for a narrow and controlled velocity distribution of the particles along with a uniform spatial distribution of those particles on the target [13].

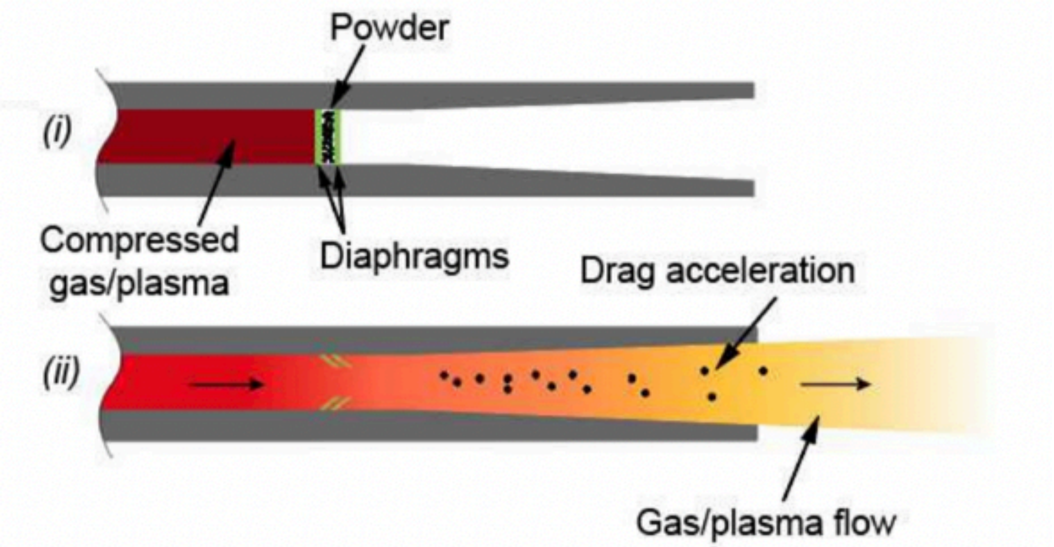

Figure 5: Two types of drag-acceleration impact devices. (i) A diaphragm-based system that holds particles and is ruptured by compressed gas flow. (ii) Particle motion in the stream of compressed gas after the diaphragm has burst. Adapted from [1]

The second type of sabot-less drag acceleration impactor utilizes the same type of compressed gas velocity stream with the difference being instead of a contained flow that is released, the gas is allowed to free flow through the barrel. The intended projectiles are then introduced to the gas flow by a secondary inlet along the barrel and flow within the gas stream into the intended target [14]. A detailed schematic is shown in **Figure 6**.

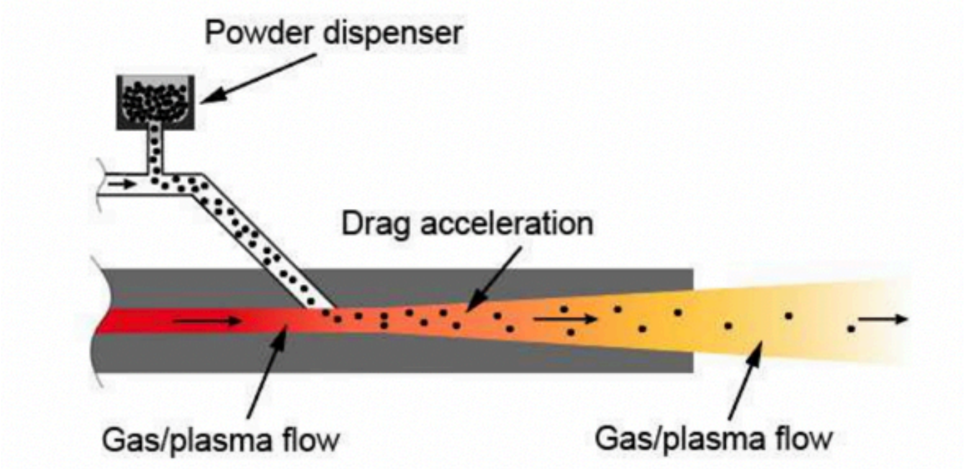

Figure 6: A different type of drag acceleration system that injects particles directly into the compressed gas flow. Adapted from [1]

These types of impact testers come with significant downsides when compared to the other impact testers detailed as part of this thesis work. The impact will only work with micron-scale particles, due to the particles having to be introduced into the compressed gas stream and needing to be light enough to be fully accelerated by the time it reaches the target. This means that a larger projectile cannot be used to simulate higher impact forces [1]. In addition, the maximum velocity of the particle is constrained to the velocity profile of the flowing gas, resulting in an uneven final velocity of the particles as well as a maximum speed of the particles equal to that of the flowing gas [15].

1.2.5 Laser Launched Flyer Plates

The next class of projectile impact testers are those based off of laser pulses to induce projectile motion. A laser launched flyer plate functions based off of laser ablation of an absorbing material. With sufficient peak laser power, the energy absorbing material, usually a transparent epoxy or other type of glue, is liquified, evaporated, sublimated, or converted to a plasma [1]. This rapid heating causes a subsequent change in volume of the material which propels the projectile towards the target much like the previous impact testing systems [16]. In the experimental setup, a laser is focused on a metallic foil that is glued upon a glass substrate. Upon the laser pulse, the glue's volume is expanded and tears a circular section of foil. This torn piece of foil becomes the flyer plate that is launched towards the target (**Figure 7**). This type of impact testing is ideal for situations where the projectile is required to be a flat, very thin piece of material that has not been deformed by traditional launch methods such as a compressed gas [17]. Like the drag-acceleration system, this type of impact tester is confined in its type of projectile with the only modifications available being the type of material the flyer plate is made of and its thickness [1].

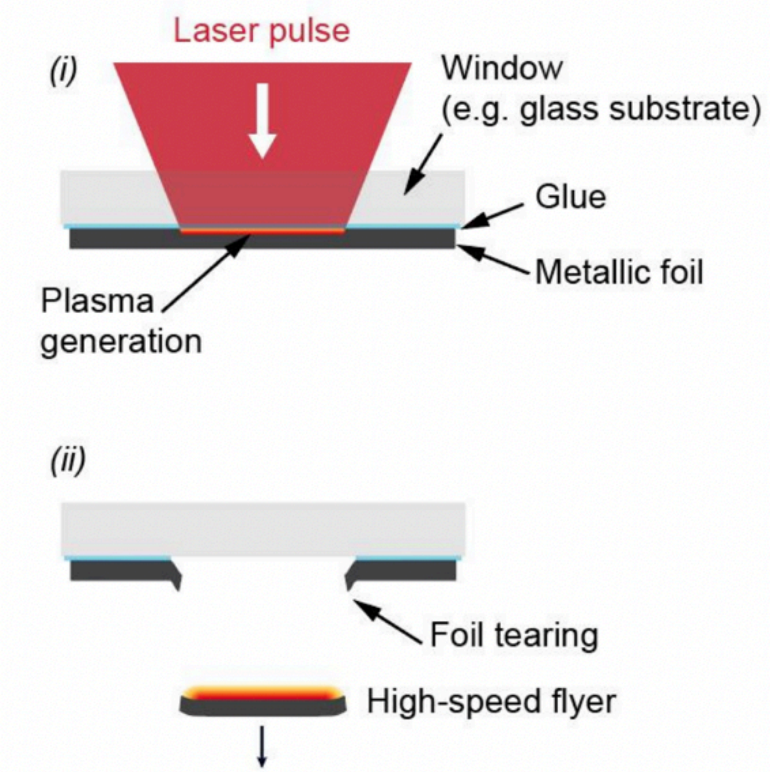

Figure 7: Laser-Launched Flyer Plate Impactor. (i) Intact metallic foil before laser firing. (ii) Laser induced flyer plate launch. Adapted from [1]

1.2.6 Laser Induced Particle Impactor

The final type of impactor that is prominent in research applications is a laser induced particle impact test (LIPIT). Much like the previous impact tester, this type of impactor is based upon laser ablation to launch a projectile towards a target sample. Unlike the previous system, LIPIT is used to launch a micron-sized particle instead of a flyer plate [1]. A laser is focused upon an ablation film and elastomer that is backed by a glass substrate. Upon laser firing the ablation film is super-heated into a plasma which expands the elastomer layer and launches the projectile (**Figure 8**). Unlike the previous types of particle projectile impact tests, the LIPIT allows for highly controlled projectile velocities as well as precise control of impact placement. This type of particle impact is restrained to very small particle impact and is therefore ideal for micro-sized experiments [18].

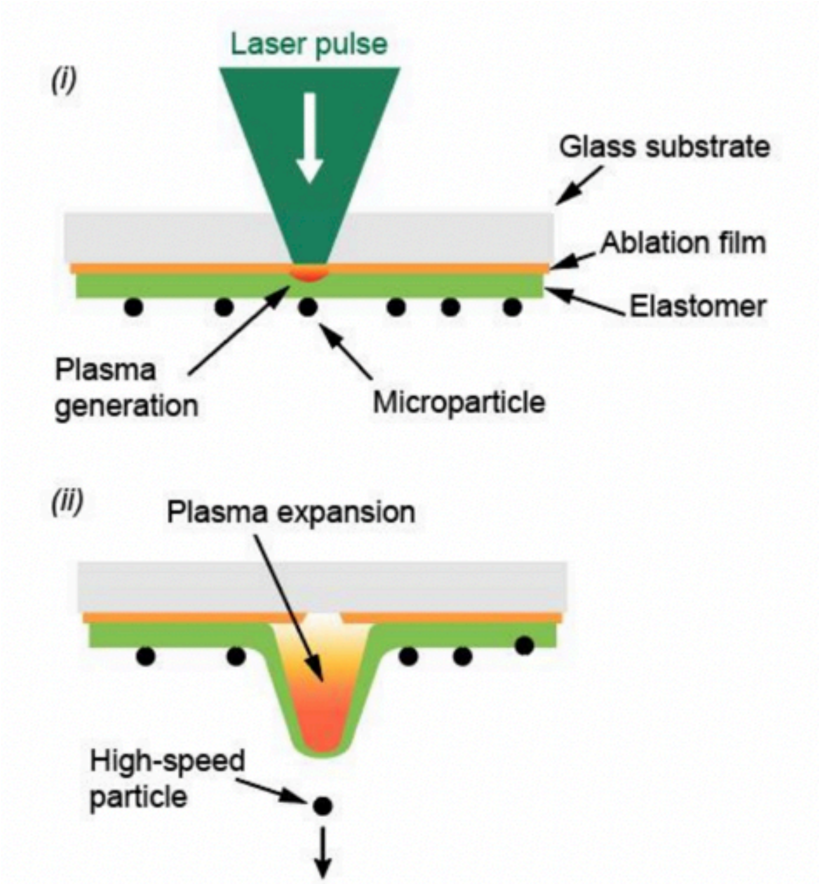

Figure 8: Laser-induced particle impact test. (i) Particles resting on substrate. (ii) Plasma expansion due to heating from laser energy. Adapted from [1]

1.3 Motivation and Thesis Contributions

The motivation for this thesis project stems from the fact that there is currently no impact tester in research that is optimized to perform at velocity ranges of 10 to 100 m/s second with projectiles on the order of several 100 microns (**Figure 1**, research gap) [1]. There are a mix of impact tests that can reach speeds over 100 m/s with projectiles of similar size ranges or testers with similar velocity ranges but much smaller projectiles, like the ones detailed in this thesis work. There is also a mix of different types of impact tests (Charpy or Izod testing) that can perform tests at lower velocities than the desired velocity range. What is needed is a projectile impactor that bridges this gap. This is especially true when testing biological materials as many of the speeds seen in nature are between the needed velocity ranges. The mantis shrimp for example, one of the fastest striking creatures in nature, has an average striking speed of 22 m/s [19]. This thesis details the design, construction, and validation of an air powered projectile impact tester that is suitable to launch projectiles that are 0.5 mm (500 microns) and smaller. The design of this tester most closely resembles that of a single-stage gas gun however it operates at a lower velocity to accommodate the needed velocity ranges for biological material testing purposes.

Chapter 2

Large Scale Proof of Concept Tester

For this project, a macro-scale projectile impact tester was built as a proof of concept for the design and construction of a micro-scale impact tester. A larger-scale tester was chosen to be built as a proof of concept to validate the design calculations and process while utilizing only off the shelf components. Using off the shelf components would drastically reduce the time to manufacture the device and the overall cost. Another benefit of the building of a larger tester is that it would provide other research members access to projectile impact testing which is not currently available at the laboratory. A design based upon a single-stage gas gun that functioned using compressed air was chosen for this impact tester due to its ease of construction, ability to fire a multitude of projectile shapes and sizes, as well as its scalability. The design goal of the final large-scale impact tester was a final velocity range of 20-50 m/s and a maximum projectile diameter of 0.25 inches. Smaller projectiles could be launched from the tester with the use of a sabot.

2.1 Design Calculations

The first step of the design process involved creating a set of design equations to determine fixed variables of the projectile impact tester such as barrel length, barrel diameter, operating air pressure, as well as air reservoir volume. A simple schematic of the design was created to visualize the numerical equations (**Figure 9**). The simplified calculations eliminate the valve and treat the expansion of the gas during firing as instantaneous.

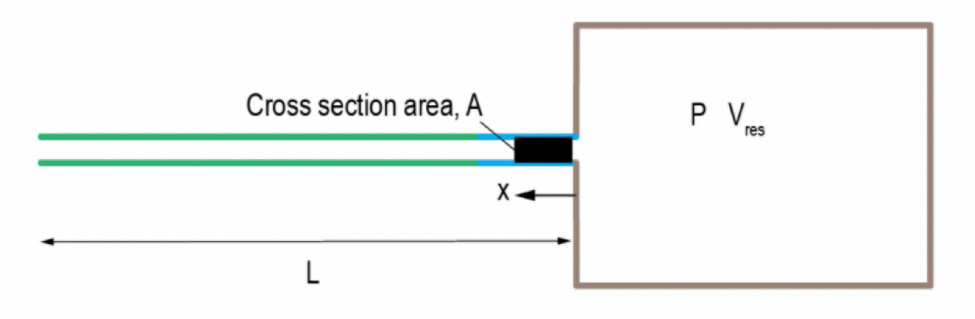

Figure 9: Simplified diagram of single-stage gas gun impact tester for calculations

An explanation of the nomenclature is outlined below:

P	Pressure
V	Volume
V_{res}	Reservoir Volume
n	Moles
R	Universal Gas Constant
A	Barrel Cross-sectional Area
x	Integration Distance
L	Length
m	Mass
v	Velocity
g	Gravitational Constant
f	Frictional Force
μ	Dynamic Friction Coefficient

The calculations started with the ideal gas law which relates the pressure and volume of a gas to the temperature and number of moles in a confined space. This was used to calculate the amount of compressed air in the reservoir.

$$PV = nRT \ \approx const \tag{2.1}$$

The volume that contains the gas however is constantly changing due to the projectile moving down the length of the barrel as it is launched. To take this into account, the cross-sectional area of the barrel multiplied by an integration variable was added to the original volume of the reservoir.

$$V = V_{res} + A \cdot x \tag{2.2}$$

The adjusted volume term was then substituted into the ideal gas equation which was rearranged to solve for pressure.

$$P = \frac{nRT}{V_{res} + A \cdot x} \tag{2.3}$$

An integral equation was created with pressure multiplied by the barrel's cross-sectional area to determine the force of the gas propelling the projectile forward. A force loss term was also placed within the integral to account for the force needed to overcome the friction of the projectile as it slides along the barrel. The limits of the integration were set to 0 and L respectively to account for the force along the entire length of the tester's barrel. Force over distance equals work which allows the equation to be equated to the change in kinetic energy of the projectile. Because the projectile starts at rest, no integration is needed for the kinetic energy term.

$$\int_0^L (PA - f)dx = \frac{1}{2}mv^2 \tag{2.4}$$

The pressure equation (2.3) was substituted into the integral along with the equation for dynamic frictional force. A dry steel on stainless steel friction coefficient of 0.57 was used throughout the design process [20].

$$\int_0^L \left(\frac{nRTA}{V_{res} + A \cdot x} - \mu mg\right) dx = \frac{1}{2}mv^2 \tag{2.5}$$

The whole equation was then rearranged to solve for the final velocity of the projectile.

$$v_f = \sqrt{\frac{2}{m}\left[\int_0^L \left(\frac{nRTA}{V_{res} + A \cdot x}\right) dx - \mu mgL\right]} \tag{2.6}$$

The final equation was optimized to produce the desired final velocity of the impact tester considering the availability of off the shelf parts as well as the maximum compressed air pressure available in the lab. The final calculated design called for a 1-gallon reservoir, a 7.5 ft long by

0.25 in diameter barrel, and a projectile mass of 0.5 oz. At a pressure of 50 Psi the resulting calculated velocity was 60 m/s which is greater than the desired final velocity.

2.2 Design and Fabrication

Before the physical build of the impact tester began, the entire system was designed using Computer Aided Design (CAD) to gain a full parts list as well as cut list of materials (**Figure 10**). CAD is a really helpful tool when constructing engineering projects as it allows for the quick iteration of designs as well as finding how each part of the project will interface with another. As stated before, the entire design was based around parts that could be easily sourced and at low cost. To this end, a stainless-steel barrel was chosen that measured 7.5 ft long with an internal diameter of 0.25 in. Stainless-steel was chosen because it is the only material available for a tube with a seamless construction. A seamless barrel is needed for this application because it means that the internal surface of the tube is completely smooth and devoid of any potential obstructions which is essential when designing a projectile launcher of any kind [21]. An industrial 1-gallon air tank was chosen as the air reservoir for this project with a maximum pressure rating of 500 Psi; more than enough for this application. The initial pressure of the system was controlled with a 0-300 Psi regulator which allowed for precise control of the pressure within the air reservoir. An air regulator with a blow off feature was specifically chosen so that the air pressure within the system could be easily increased or decreased by turning a knob. The pressure of the system was measured using a laboratory grade pressure gauge and a quick opening solenoid valve was used as the firing mechanism for the tester. A signal would be sent to the solenoid, introducing the compressed air in the reservoir to the barrel, and the projectile would be launched. Also included in the design was a containment box at the end of the tester to house the target sample. The purpose of this box was to contain the entire impact event so that no fragment of either the projectile or the target could escape and potentially injure researchers. The final major component of the design was an aluminum stand made out of T-slot rails to mount all of the parts to. T-slots rails were used due to their modular nature so that equipment could be added or removed quickly and easily to facilitate whatever the experiment required at the time. Presented in **Figure 11** is a detailed photo of the completed large-scale tester with important components highlighted. An expanded view of the air system of the impact tester is shown in **Figure 12.**

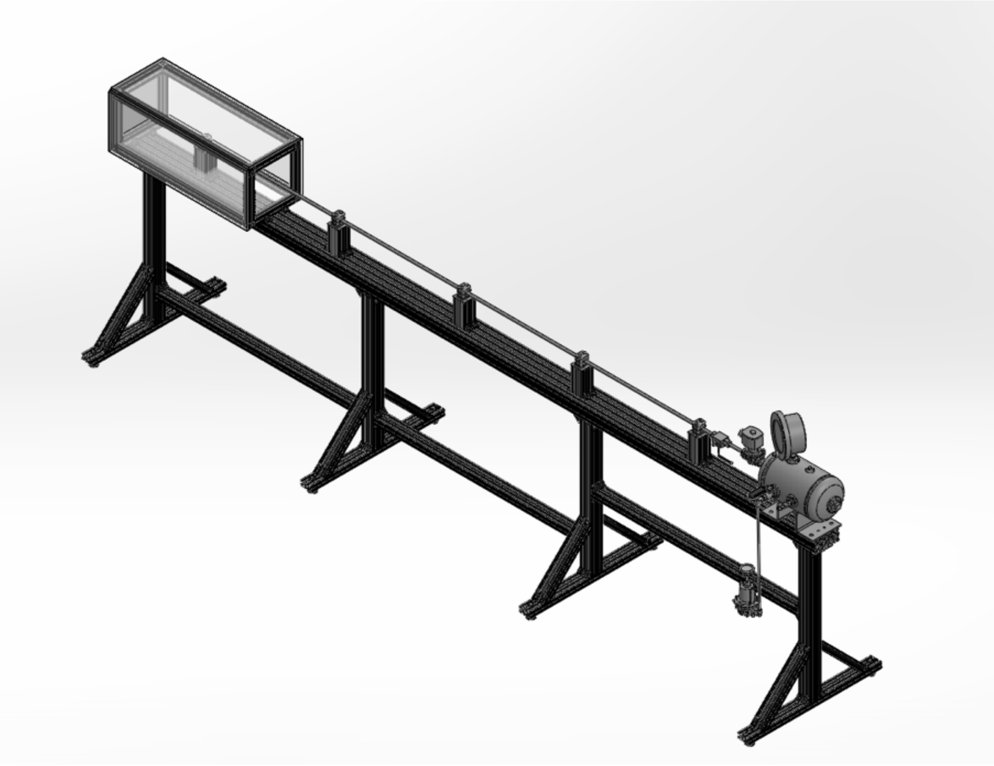

Figure 10: Final CAD design of large-scale projectile impact testing device

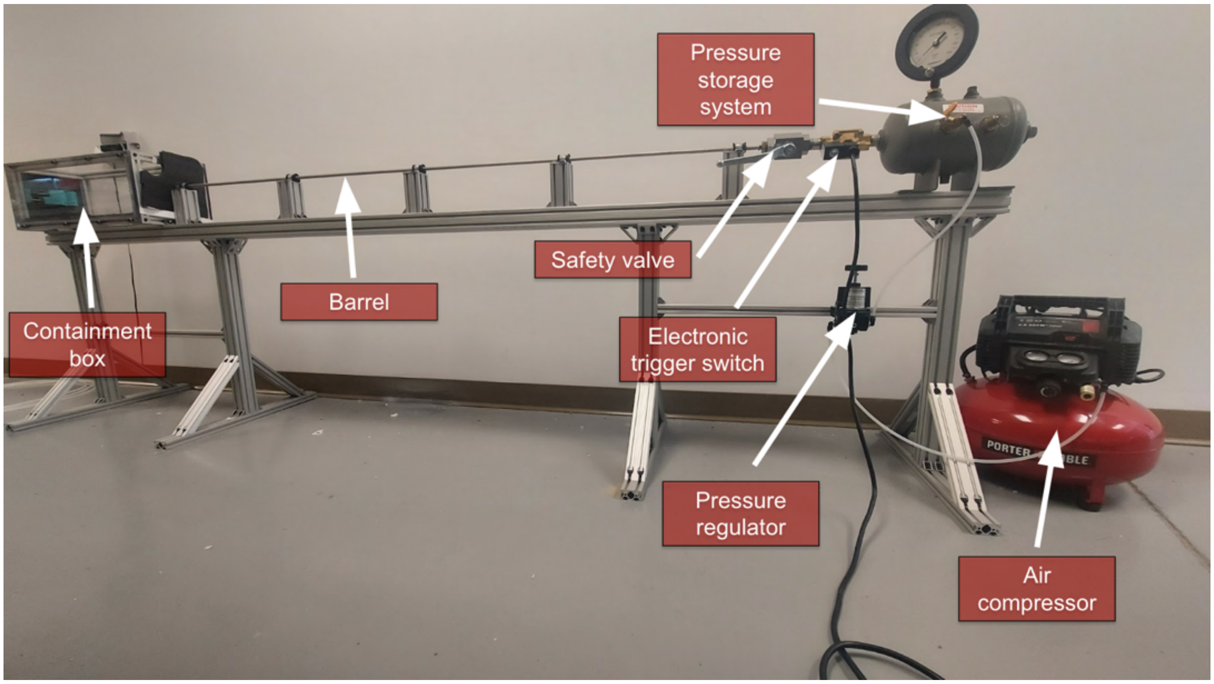

Figure 11: Completed impact tester with important components highlighted

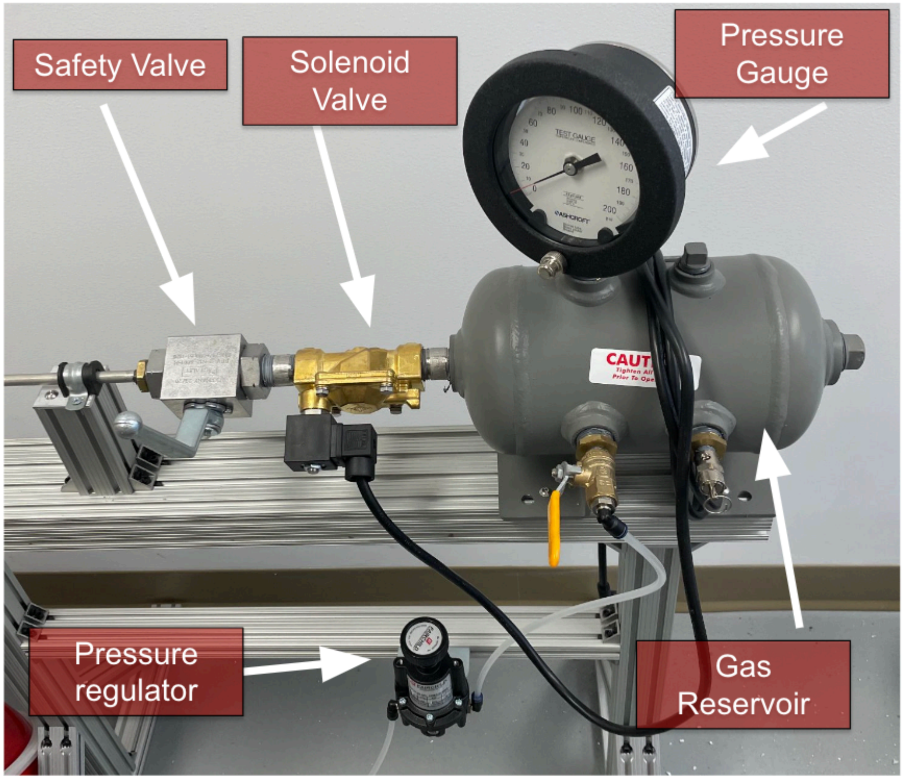

Figure 12: Air system components of large-scale impact tester

All of the materials for the tester were sourced per the CAD design with the aluminum pieces being the only parts that had to be cut to length. Once the device was assembled, an analog push button switch was integrated into the system to act as a firing mechanism. A simple chronograph placed at the end of the barrel and before the target was used to measure the velocity of the projectile.

2.3 Design Validation and Testing

A relationship between the pressure and velocity had to be created before any firing of samples could take place. This was to create an equation to determine the velocity of the projectile when the tester was charged to a certain pressure as well as to insure the repeatability of the chosen velocity. A benefit of this was that the accuracy and precision of the projectile could also be quantified. For this validation test, a 0.25 in ball bearing was used as the projectile and fired three times at a specific Psi range. The Psi range was then changed and the test repeated. A velocity curve for the tester was determined using the variation in psi and the measured velocity of the projectile. The data for these tests is tabulated in **Table 2** with a graph given in **Figure 13**.

Table 2: Pressure vs velocity for large-scale tester validation tests

Pressure (Psi)	Test 1 Velocity (m/s)	Test 2 Velocity (m/s)	Test 3 Velocity (m/s)	Avg. Velocity (m/s)	Standard Deviation
5	*39.2*	*39.1*	*38.4*	*38.90*	*0.44*
10	*56.3*	*57*	*56.3*	*56.53*	*0.40*
15	*67*	*68*	*68.8*	*67.93*	*0.90*
20	*80.9*	*80.8*	*80.8*	*80.83*	*0.06*
25	*89.8*	*88.7*	*88.9*	*89.13*	*0.59*
30	*96.4*	*96.6*	*93.8*	*95.60*	*1.56*
35	*103.9*	*102.5*	*103.5*	*103.30*	*0.72*
40	*109.3*	*107.4*	*108.7*	*108.47*	*0.97*
45	*115.2*	*116*	*115*	*115.40*	*0.53*
50	*117.8*	*118.6*	*118.2*	*118.20*	*0.40*
55	*120.5*	*121.5*	*121.1*	*121.03*	*0.50*
60	*125.5*	*124.1*	*125.3*	*124.97*	*0.76*
65	*128.3*	*128*	*125.9*	*127.40*	*1.31*
70	*134.7*	*132.5*	*133.3*	*133.50*	*1.11*
75	*136.8*	*135.8*	*135.5*	*136.03*	*0.68*
80	*137.5*	*137.3*	*139*	*137.93*	*0.93*

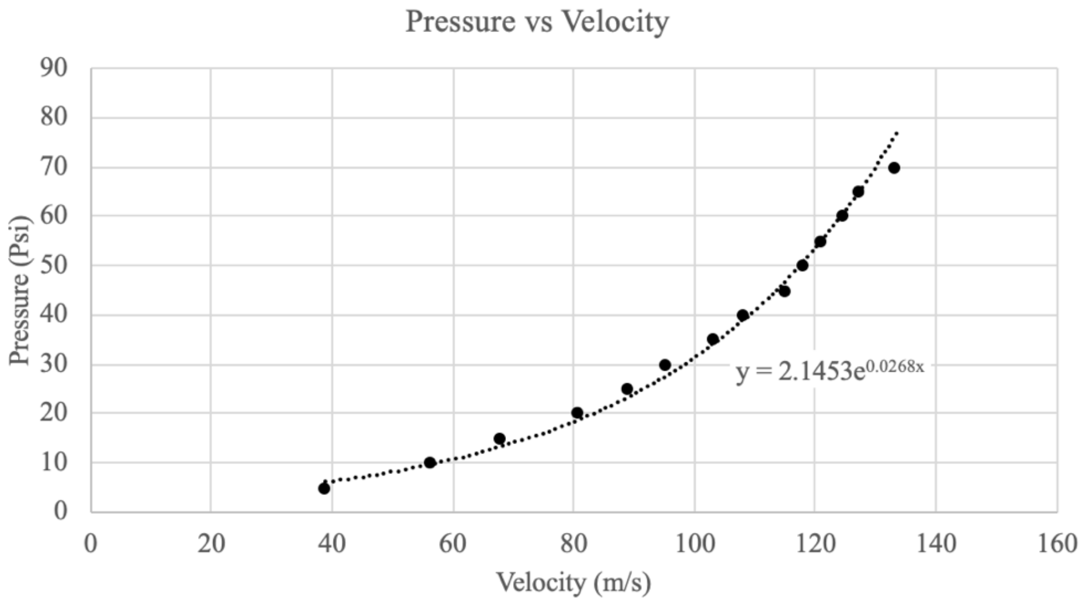

Figure 13: Pressure vs. velocity data for large-scale impact tester with trend line

The resulting average standard deviation for the three tests at each Psi setting was 0.74 m/s which proves that the desired impact velocity of the tester is highly repeatable. Included in the graph is an exponential trendline to fit the data along with its corresponding equation (2.7). An important note is that to build the correct format of equation, the velocity was plotted on the X axis with the reservoir pressure plotted on the Y axis, even though the velocity is actually a function of the pressure. This allows the user to enter in a desired projectile velocity and solve for a corresponding pressure to calibrate the system to.

$$P_{res=2.1453e^{0.0268\cdot v_f}} \tag{2.7}$$

The resulting R^2 value of 0.9895 suggests a very accurate correlation between the desired final velocity and the initial pressure of the reservoir. The characterization of the velocity curve also allowed for a measure of the accuracy and precision of the device. After three tests of each pressure setting, the projectile struck the same impact crater on the sample target used for the validation process with any difference in placement being negligible which correlates to excellent precision. A laser level was utilized to align the barrel with the target and utilized again at the end of the test to ensure that the projectile struck the correct location. Again, there was negligible difference in the final impact crater and the planned impact location which confirms the device's accuracy.

Included in **Figure 14** for a visual representation of the impact crater is a series of bio-inspired cement-polymer composite samples that were subjected to impact testing. A 0.25-inch diameter round projectile was used for these particular impact tests with the impact craters highlighted in red. These tests were conducted by a researcher in Virginia Tech's Biological and Bio-Inspired Materials Lab during an ongoing investigation into the impact resistant properties of controlled orientation prismatic rods in bio-inspired composites.

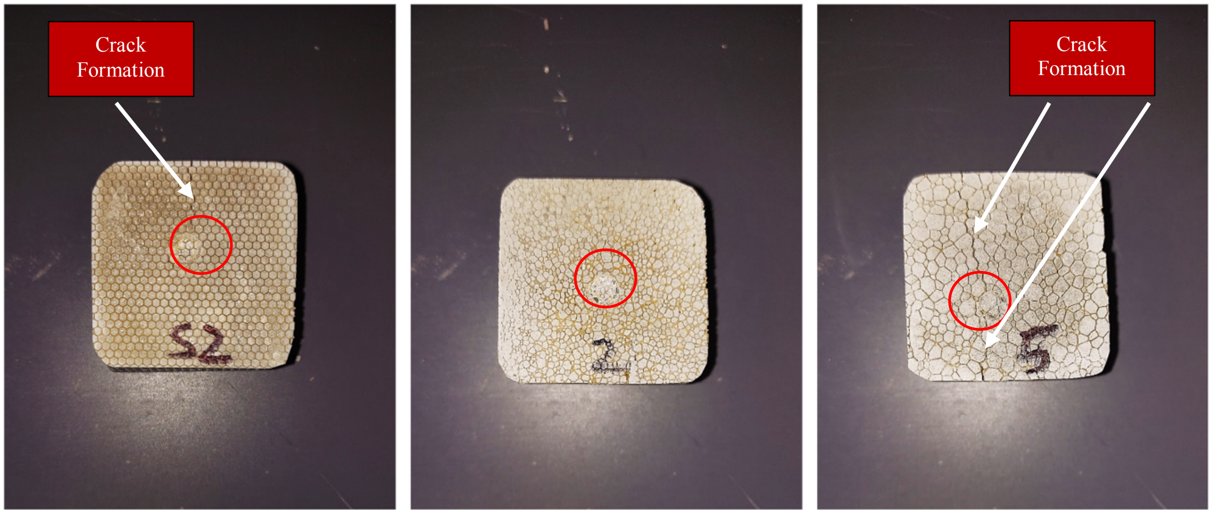

Figure 14: Representation of bio-inspired composite with impact crater of 0.25-inch round projectile highlighted in red.

Chapter 3

Micro-Scale Impact Tester

After the validation of the large-scale tester, work could begin on the micro-scale projectile impact tester. The design of this tester was driven by the lessons learned while fabricating and operating the large-scale version, with many of the larger components remaining the same. The specific design criteria of this system were a velocity range of 20-50 m/s second with a projectile size of 0.5 mm.

3.1 Design Calculations

The same equations that were used to choose the characteristics of the large-scale device were also utilized to design the smaller version. The same integral was used with the force due to the expanding air volume being offset by the force of friction of the projectile moving down the barrel. This was equated to the kinetic energy change of the projectile and arranged to solve for final velocity of the projectile.

$$v_f = \sqrt{\frac{2}{m}\left[\int_0^L \left(\frac{nRTA}{V_{res} + A \cdot x}\right) dx - \mu m g L\right]} \tag{3.1}$$

The final velocity equation (3.1) was constructed in Microsoft Excel to act as optimization software and the initial fixed values were entered in. These fixed values included the 0.57 friction coefficient [20], a reservoir volume of 1 gallon, and a maximum pressure of 160 Psi. The calculated design called for an initial barrel length of 0.5 m, a barrel diameter of 0.5 mm along with an initial reservoir volume of 1 gallon. This would result in an impact tester that could fire a 0.5 mm (500 micrometer) projectile within the desired speed range of 20 – 50 m/s.

3.2 Design and Fabrication

The entirety of the projectile impactor system was modeled using CAD software to ensure all of the parts interacted correctly and as a reference for sourcing components. Unlike the large-scale version, the smaller impactor needed several of its parts to be custom machined due to the extremely small nature of the desired projectiles, making the use of CAD software essential. Machined components include the connection between the barrel and the gas reservoir, the sample holder for materials' tests, as well as barrel shrouds. The barrel shrouds are two pieces of aluminum that surround the fragile 0.5 mm diameter barrel so that it does not bend or distort during firing or transport of the system (**Figure 15**). The barrel itself for the micro-impact tester is a piece of 0.5 mm internal diameter stainless steel tubing that has a manufacturer applied silicon coated interior. A silicon coating was chosen for this application to reduce damage to the barrel during long term use of the device. It is important to note that the silicon coating does not reduce the overall internal diameter of the tube as the tube is manufacture oversized and the built-up coating brings the tube into desired specifications.

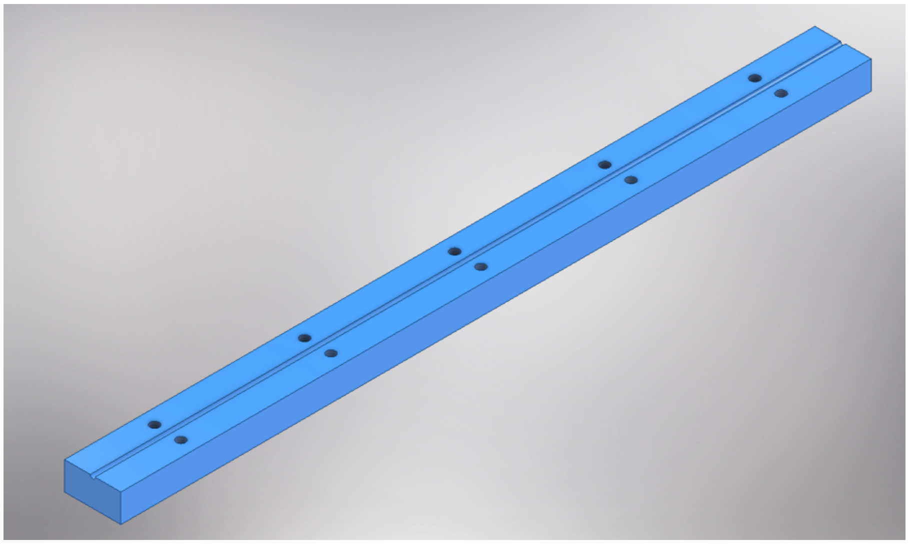

Figure 15: CAD image of aluminum barrel shroud half

The same air reservoir, gas gauge, and pressure regulator were used in this design due to their excellent performance as part of the macro-scale system. They were consistently able to hold a constant pressure and repeatedly fire at the same velocity. The same style of solenoid valve was utilized in this design as the previous however it was sized appropriately for the smaller scale

(**Figure 16**). A valve with a flow coefficient (C_v) of 0.21 and operating range of 0 to 500 Psi was chosen for this application. The flow coefficient characterizes a valve's ability to flow gas or liquid through its orifice and needs to be sufficiently large to provide near instantaneous release of as much gas as possible to insure maximum energy transfer from the compressed gas to the projectile before it leaves the barrel.

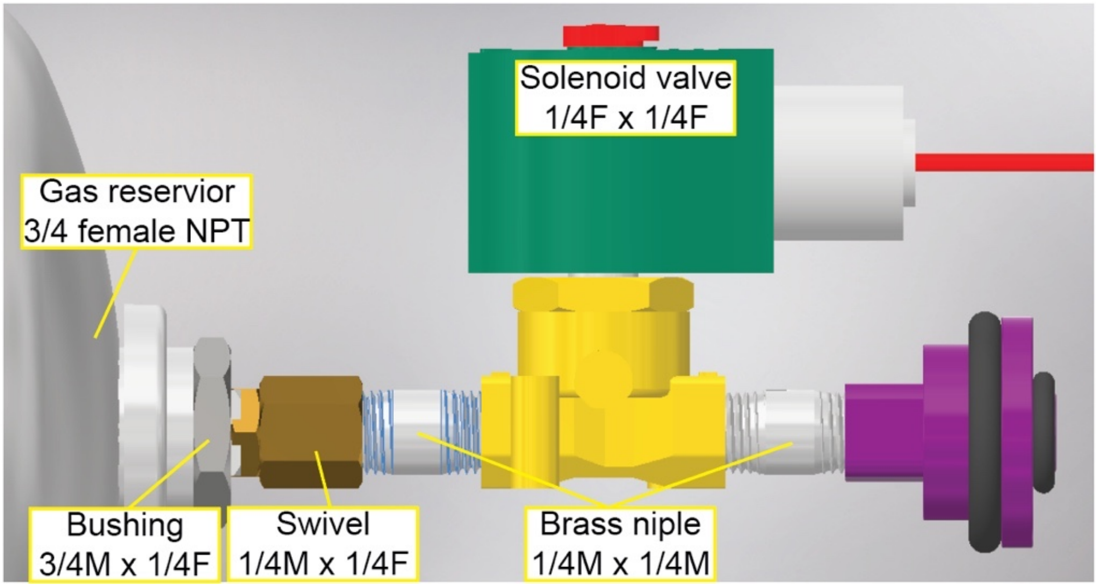

Figure 16: CAD image of connection between gas reservoir (grey), solenoid valve (green), and barrel connection (purple).

One deviation from the previous design was the addition of a breech mechanism between the solenoid valve and the barrel of the tester. A lesson learned from the larger tester is that it was cumbersome to 'muzzle-load' the projectile every time for a shot. To load a projectile into the large impactor, the user had to first place the projectile into the end of the barrel and then use a long flexible piece of plastic to push the projectile to the start of the barrel close to the valve. The addition of a breach, known as a wraparound breach in this application, allows for a projectile to be easily loaded into the barrel without having to disassemble the sample chamber [22]. A user only has to unscrew the connection between the solenoid valve and the barrel to load a projectile; a much easier and less cumbersome loading process. The breach is double O-ring sealed to ensure no leakage of pressure and complete transfer of energy to the projectile (**Figure 17**). The breach design required that the air reservoir be mounted on linear guide rails to facilitate its opening and loading of a projectile because a gap between the two sides of the connection needed to be present to fit the projectile into the barrel.

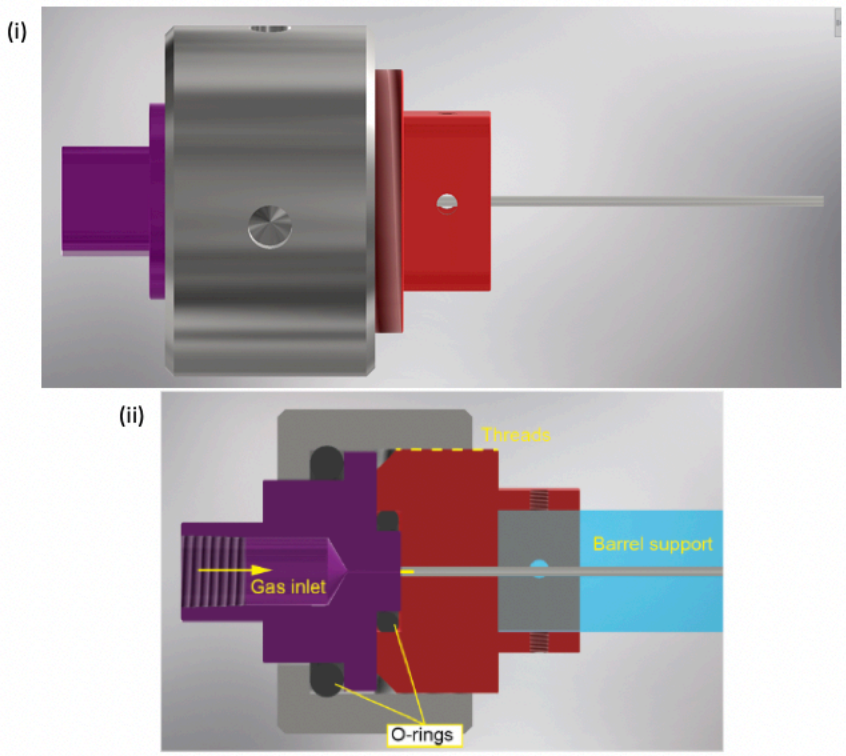

Figure 17: CAD image of breach design. (i) Complete view of breach. (ii) Cross-section view to show internal structure of breach.

To accommodate small target samples and to insure accurate projectile impacts, a sample holding system was devised to correctly align and securely hold targets. The designed holder consisted of a block of steel mounted on linear motion shafts. These linear shafts were in turn mounted to the sample chamber front wall and barrel connection flange as seen in **Figure 18,i**. A design consisting of linear shafts was chosen to accommodate samples of varying sizes while retaining a consistent alignment to the end of the barrel; the sample plate could be moved closer or further away from the barrel without changing the horizontal or vertical location. The sample plate itself was machined with a reference pattern to allow for precise placement of the target sample (**Figure 18,ii**). The center of the cross pattern represents direct alignment with the end of the barrel. Much like the large-scale impactor, the micro-scale tester included a sample chamber constructed out of T-slot aluminum rails. T-slot rails were chosen for this application to provide numerous mounting options for various vices and clamps to hold samples during experiments in which the designed sample holding system is not used. The front wall of the chamber is a machined aluminum plate to provide mounting for the barrel end mount flange and the linear guide rails while the rear of the chamber is a steel plate to ensure that if a projectile where to travel all the way through a target sample it would have a solid backstop. The other faces of the sample chamber consist of 0.5-inch polycarbonate. Polycarbonate is a clear, impact resistant plastic that was chosen to provide adequate protection from deflected projectiles and sample fragments while also providing an unobstructed view of the impact event.

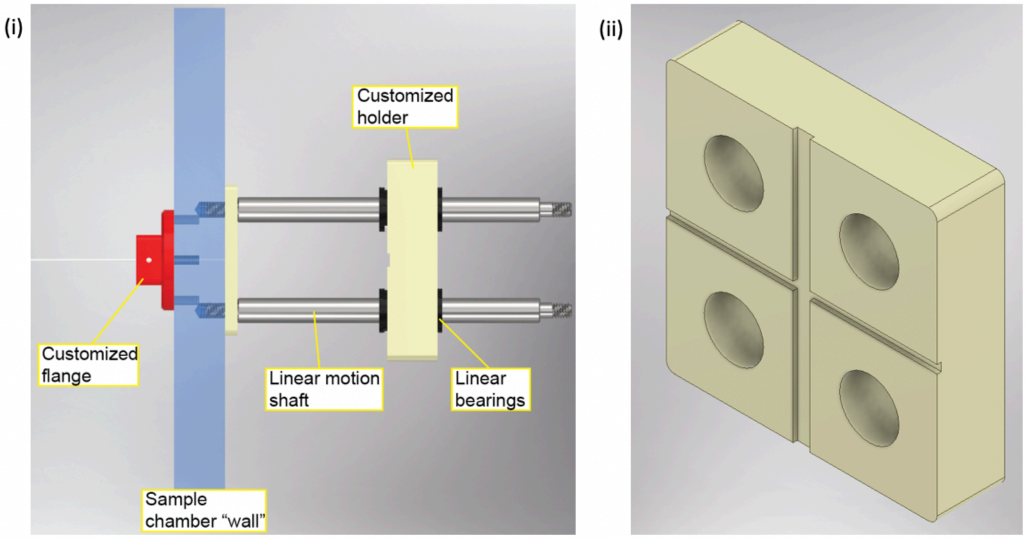

Figure 18: (i) CAD image of target sample holder system. (ii) Sample holder plate with target alignment pattern

Figure 19 details the entire CAD design of the micro-impact tester with all of the major components highlighted. This image was used during the construction of the device to accurately assemble the entire tester. An important note, instead of resting on an aluminum stand, this impactor was designed to be affixed to a fixture table with a 1.5 x 1.5 in bolt hole grid. This design choice was made so that the design is easily reconfigured for different types of experiments as well as being able to be setup at different research institutions for various experimental conditions.

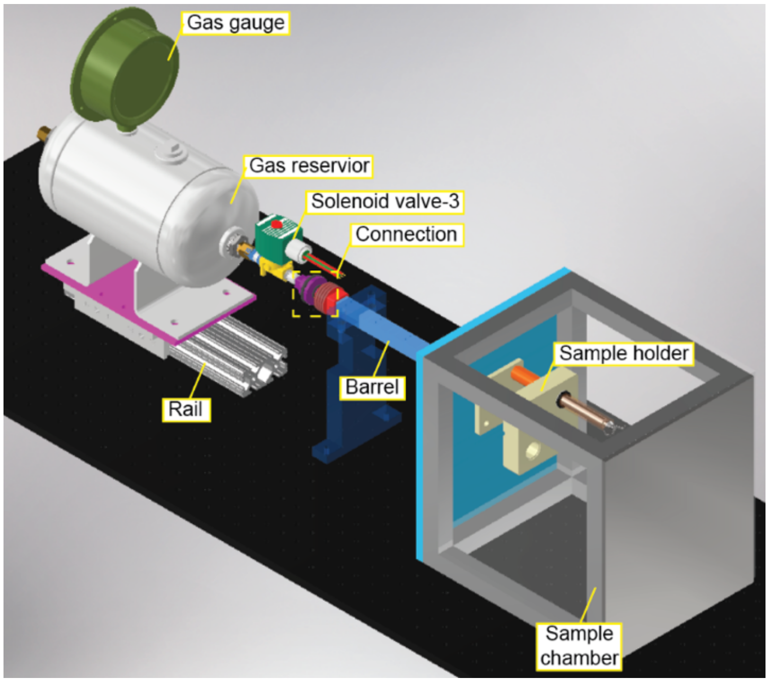

Figure 19: Final CAD design of micro-scale projectile impact tester

Presented in **Figure 20** is the completed micro-impact tester with significant components highlighted. Similar to the proof-of-concept device, the small-scale device was built to the initial CAD specifications with no revisions needing to be made.

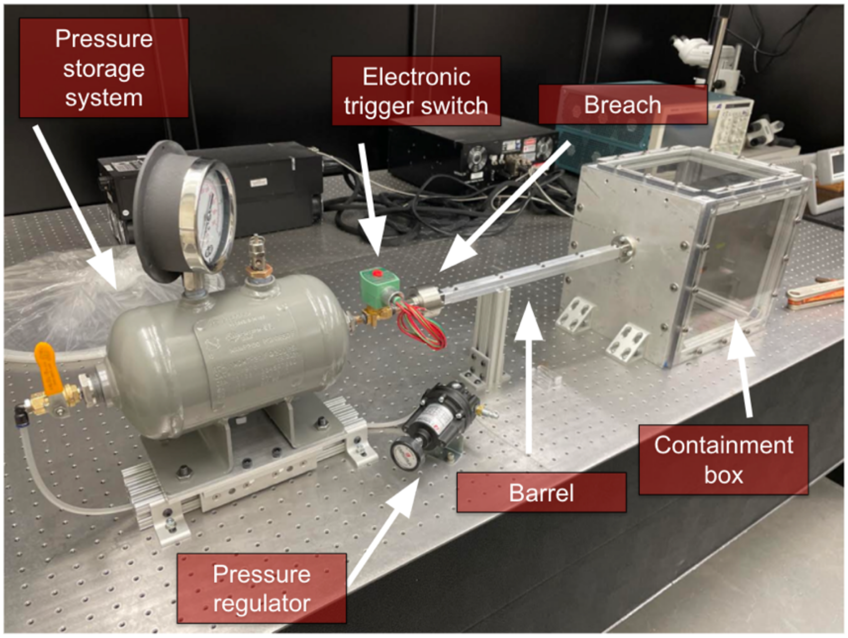

Figure 20: Completed micro-impact tester with important components highlighted.

A zoomed in view of the specific connection between the gas reservoir, solenoid valve, breach, and barrel is provided in **Figure 21**. As per the CAD design, a reducing connection was used to step down the ¾ inch NPT outlet of the gas reservoir down to the ¼ inch NPT inlet size of the solenoid. Two ¼ inch NPT brass nipples were used to connect both the gas reservoir to the valve and the valve to the breach. The breach itself was then connected to the barrel located within the barrel shroud.

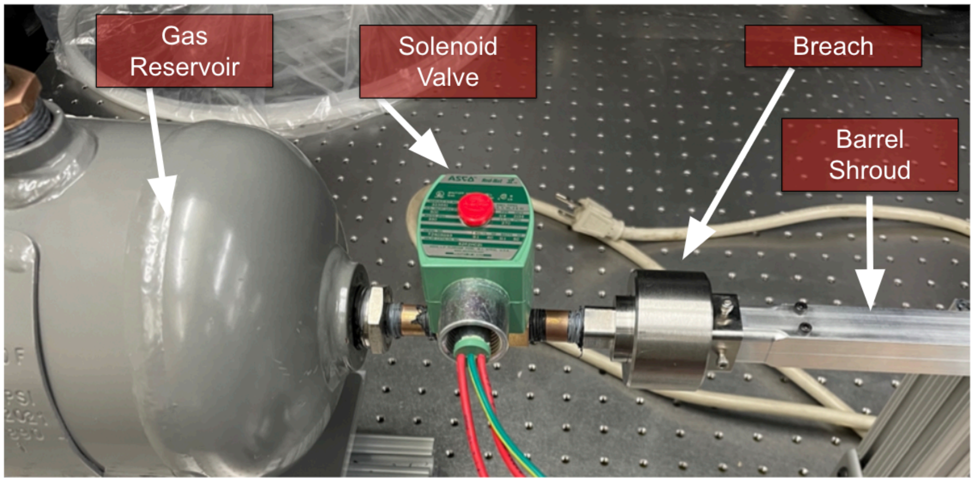

Figure 21: Completed connection between gas reservoir, solenoid valve, breach, and barrel

Another major difference between the large-scale impactor and the micro-scale version is the firing control of the device. Instead of using an analog push button switch to control the firing, the micro tester is controlled with an Arduino, a microcontroller, and a 5v relay module. This change was implemented to have precise control of the firing action of the tester; the valve can be programmed to open for a specific amount of time. This ensures that the projectile movement is not influenced by excessive air flow while it is free flying in the sample chamber towards the target. Another reason for the Arduino is it allows for a timing signal to be simultaneously sent to an outside piece of equipment such as a high-speed camera or x-ray diffraction machine, two important data collection methods for micro projectile impact testing [23]. The code for the Arduino control is presented in **Figure 22**. The system relies on a simple loop that monitors the input voltage coming from the monetary push button. When the push button is pressed, the input voltage value changes and a signal is sent to the relay module to open the valve.

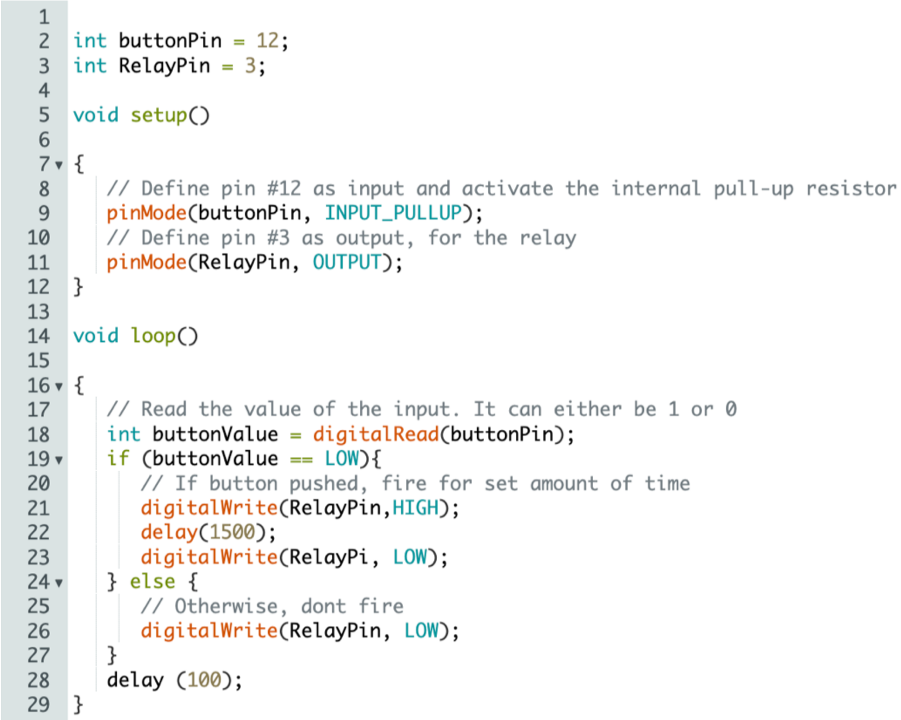

```

int buttonPin = 12;
int RelayPin = 3;

void setup()

{
    // Define pin #12 as input and activate the internal pull-up resistor
    pinMode(buttonPin, INPUT_PULLUP);
    // Define pin #3 as output, for the relay
    pinMode(RelayPin, OUTPUT);
}

void loop()

{
    // Read the value of the input. It can either be 1 or 0
    int buttonValue = digitalRead(buttonPin);
    if (buttonValue == LOW){
        // If button pushed, fire for set amount of time
        digitalWrite(RelayPin,HIGH);
        delay(1500);
        digitalWrite(RelayPi, LOW);
    } else {
        // Otherwise, dont fire
        digitalWrite(RelayPin, LOW);
    }
    delay (100);
}
```

Figure 22: Control code for Arduino firing control

3.3 Velocity Measurement Issues

The original plan for the micro projectile tester was to utilize a through-beam optical sensor to detect the projectile as it exited the end of the barrel of the device. A through-beam optical sensor is a type of photoelectric sensor that utilizes an infrared laser and an optical sensor to record an event that either breaks the laser beam and when the beam becomes uninterrupted [24]. A schematic of this process is shown in **Figure 23** [25]. The sensor was put at the end of the barrel and was broken when the projectile passed through the sensor. The time of the rising signal of the projectile breaking the beam was compared to the time of the falling signal as the beam became continuous again using a Raspberry Pi Pico microcontroller module in conjunction with a computer running Python. The edges of these rising and falling signals were what was scanned for using the microcontroller to achieve the most efficient detection of the projectile [26]. The length of the projectile could then be divided by this time to calculate the velocity.

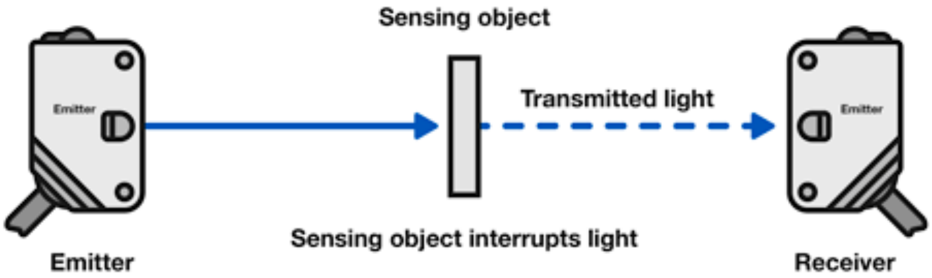

Figure 23: Through-beam optical sensor operation schematic. Adapted from [25]

Unfortunately, the timing resolution of the sensor was not quick enough to sense the projectile flying through the laser beam. Before the purchase of the specific through-beam sensor, simple motion calculations were performed to make sure that the resolution of the sensors were small enough to actually detect the projectile. However, the real-world testing of these sensors did not line up with the expected results. The system was able to determine the velocity at lower speeds however when the pressure of the system was increased, the system could not detect the projectile flying through the sensor beam.

To fix this issue, the through-beam sensors were removed and instead a high-speed camera was used to take a video of the projectile as it leaves the end of the tester's barrel. The video for an event was analyzed and the number of pixels that the projectile takes up was determined as well as the pixel location of the tip of the projectile. The video was then advanced a set number of frames and the new pixel location of the tip was recorded. By knowing the ratio of the pixel length of the projectile, the number of pixels that the projectile moved during the set number of frames, and the frame rate of the camera (10488 fps), it is a simple calculation to find the velocity of the projectile [27, 28]. An example of the projectile moving during still frames of a slow-motion video for an impact event is shown below in **Figure 24**. This method was not the original method for determining the velocity of the moving projectile but it is just as effective to determine the velocity of the projectiles.

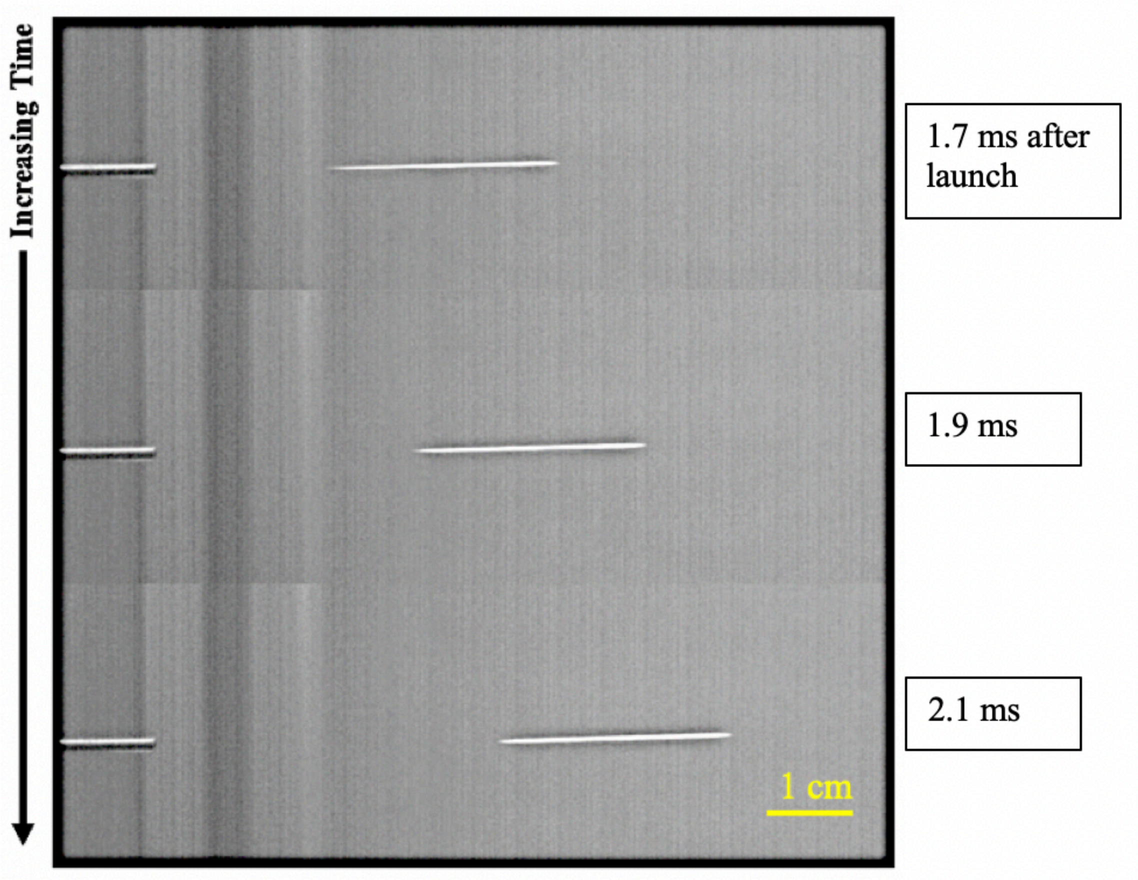

Figure 24: Slow-motion camera images of projectile motion during impact event

3.4 Design Validation and Testing

Similar to the proof of concept tester, the validation for the micro-scale launcher consisted of mapping out the specific pressure vs velocity curve of the tester. A 0.5 mm diameter projectile with a length of 22.5 mm was utilized for this validation. The projectile was fired three times at different reservoir pressures into a simulated target and the velocity for each test was recorded for each event (**Table 3**). From the multiple tests the average of each velocity was calculated to facilitate a velocity curve for the tester. An average standard deviation across the various calibrated pressures was 0.75 m/s, suggesting that the tester is highly repeatable. The resulting data was then plotted and a trend line was fitted to determine the specific pressure needed for a specific velocity (**Figure 25**).

Table 3: Pressure vs velocity for micro-scale tester validation tests

Pressure (Psi)	**Test 1 Velocity (m/s)**	**Test 2 Velocity (m/s)**	**Test 3 Velocity (m/s)**	**Avg. Velocity (m/s)**	**Standard Deviation**
30	*22.04*	*23.4*	*23.5*	*22.98*	*0.82*
40	*27.6*	*27.09*	*28.05*	*27.58*	*0.48*
50	*31.15*	*31.89*	*30.62*	*31.22*	*0.64*
60	*33.95*	*35.02*	*34.47*	*34.48*	*0.54*
70	*36.23*	*37.23*	*35.83*	*36.43*	*0.72*
80	*37.85*	*40.7*	*39.11*	*39.22*	*1.43*
90	*41.11*	*41.58*	*42.53*	*41.74*	*0.72*
100	*42.6*	*44.33*	*42.37*	*43.1*	*1.07*
110	*45.08*	*45.9*	*44.47*	*45.15*	*0.72*
120	*47.1*	*47.88*	*46.62*	*47.2*	*0.64*
130	*49.24*	*50.01*	*49.43*	*49.56*	*0.40*
140	*49.9*	*50.55*	*50.39*	*50.28*	*0.34*
150	*51.64*	*52.8*	*51.2*	*51.88*	*0.83*
160	*52.94*	*54.41*	*52.1*	*53.15*	*1.17*

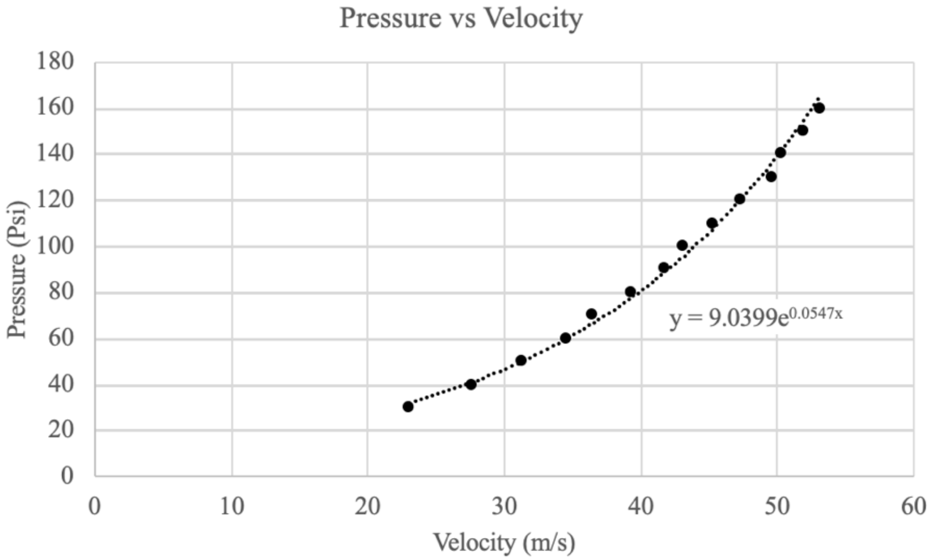

Figure 25: Pressure vs. velocity data for micro-scale impact tester with trend line

The data was plotted with the velocity as the independent variable and the pressure as the dependent variable. This is opposite of the real-world nature of the impact tester because the final projectile velocity is dependent upon the initial pressure in the air reservoir. However, the resulting equation from the trend line of the switched X and Y axis allows a user of the tester to input the desired velocity into the equation and solve for the exact pressure that the tester needs to be calibrated to.

$$P_{res=9.0399e^{0.0547\cdot v_f}} \tag{3.2}$$

The resulting exponential equation (3.2) closely follows the data with an R^2 value of 0.9956. This corroborates the visual assumption that the trend line accurately characterizes the data. The required initial reservoir pressure, P_{res}, can be found by inputting the needed final velocity, v_f, of the projectile.

The validation tests of the small-scale impact tester also included a measurement of the accuracy and repeatability of projectile impact location. Across the various impact velocities, there was a negligible amount of deviation in the impact location with the projectile consistently entering the same impact crater on the backstop target used during the validation process.

Chapter 4

Current Lab Use Case

To demonstrate that the micro-scale projectile impact tester is a viable research tool to analyze small samples and to show its usefulness, in particular when investigating biological materials, a short study of the impact properties of sea urchin spines was conducted.

4.1 Impact Properties of Biological Ceramic Foams

Foams have long been shown to have excellent impact absorption characteristics due to the nature of their porous structure. The deformation mechanisms of the cells allow the foam to disperse the energy of the impact such that the maximum impact energy is kept under a certain threshold [29]. In many cases, the impact energy seen by a foamed material is well below that of the same non-foamed version of the material [29]. This concept can be applied to brittle materials as well, usually in the form of ceramics. These ceramic foams are made up of fused-together ceramic particles that form complex, three-dimensional porous structures [30]. Studies show that ceramic foams have excellent energy and wave absorption capabilities and are often utilized in impact resistant applications due to their excellent shock absorption properties and unique combination of low density and high stiffness [30, 31]. A major drawback of ceramic foams is their inherently brittle nature. Even though they show excellent impact energy absorption properties, they dissipate this energy by breaking apart and compacting into the impact zone [31]. However, this effect is not widely studied in naturally forming ceramic foams. To this end, the hope is to use a biological ceramic foam, that of sea urchin spines, as a model system to evaluate a natural ceramic foam's impact resistance.

Sea urchins have numerous long thin spines making up their endoskeleton structure which provide the animal with functions such as locomotion, sensing, and protection against predators [32]. The internal microstructure of these spines is a porous single-crystal made of a ceramic calcite mineral (**Figure 26**) [33]. Current research of the foam-like microstructure of sea urchin spines show that they have remarkably high strength and energy absorption capabilities due to the ultra-low stress concentrations within the microstructure during loading [33]. Analysis of the internal microstructure demonstrates that the crystalline morphology of the sea urchin spine, despite the brittleness of its calcite constituent material, results in a strong, stiff, and lightweight material [32]. This unique morphology makes the sea urchin spine a perfect candidate for modeling the impact resistant behavior of brittle ceramic foams and to prove the validity of this thesis project.

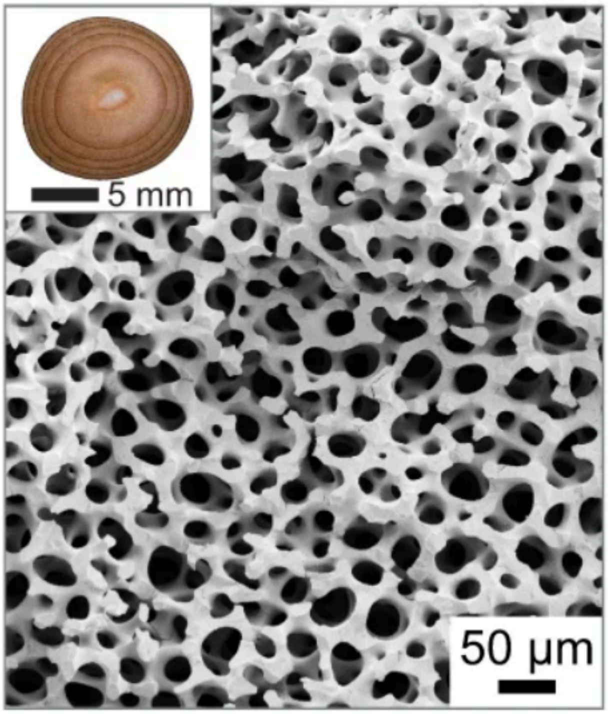

Figure 26: SEM image of porous micro-structure of sea urchin spine. Adapted from [33]

4.2 Testing of Impact Properties

For this test, *Heterocentrotus mamillatus* sea urchin spine samples were used. To test the impact properties of the sea urchin spines, they were first cut down into manageable sample sizes. A saw was used to cut the samples into cross sections of between 1 cm and 1.5 cm in diameter and 1 cm long. The samples were subsequently cleaned thoroughly to remove all dust and contaminants. For this test, 20 samples were prepared with the four most uniform chosen to actually be fired upon, ensuring an accurate baseline to compare results (**Figure 27)**.

Figure 27: Sea urchin spine cross-section samples

After preparation, each sample was loaded into a vise that was placed within the sample chamber of the micro-impact tester. The vise used to hold each sample had a register mark that was aligned with the barrel, which in turn allowed for the samples to be aligned properly for each test (**Figure 28**). The register mark in the vise made sure that the projectile would hit exactly in the center of the sample for each test.

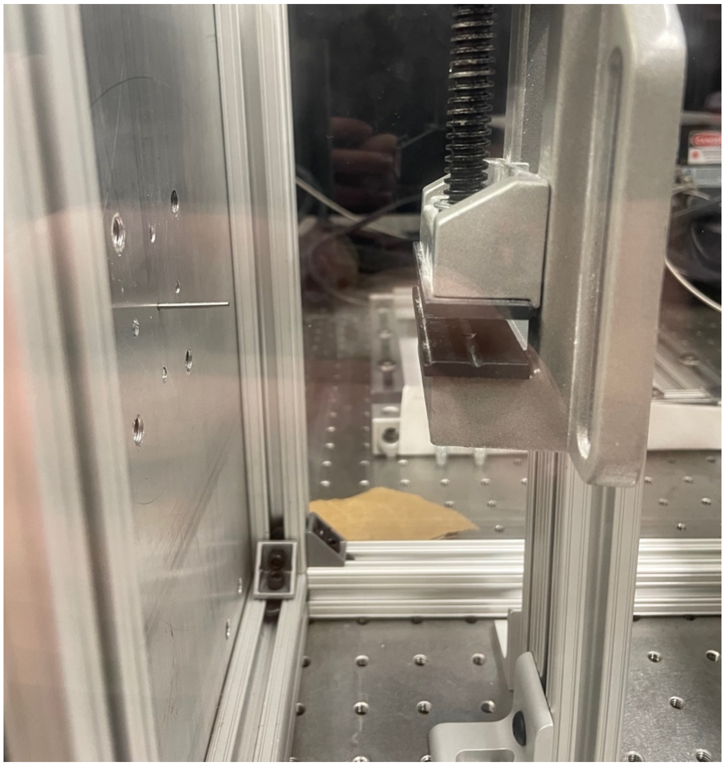

Figure 28: Sample holding vise for sea urchin spine impact tests

A 0.5 mm diameter by 22.6 mm long H2 tool steel projectile was utilized for the impact test with a mass of 3.61E-05 Kg. The projectile had a flat circular tip for this particular impact test. Impact velocities of 20 m/s, 30 m/s, 40 m/s, and 50 m/s were chosen for this study to test the full range of capabilities of the system and to investigate the impact properties of the sea urchin spines under various dynamic impact loading conditions. The resulting impact craters are shown in **Figure 29**. For all four impact speeds listed, the projectile came to rest in the sample material with no projectile rebounding or other damage being observed. For each of the four impacts, the projectile was fired at the center of the spine.

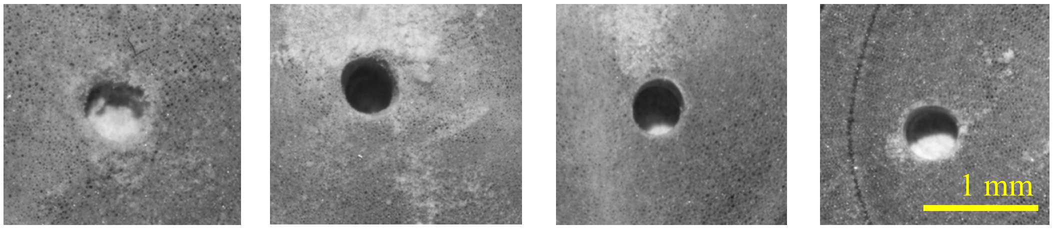

Figure 29: Sea urchin spine impacts in increasing velocity from left to right. 20m/s, 30 m/s, 40 m/s, and 50 m/s respectively.

4.3 Analysis of Impact Results

After the conclusion of the impact tests, a short analysis was performed on the samples to substantiate the use of the impact tester in the study of the sea urchin spines. The data is charted in **Table 4** below. The impact depth of the projectile was measured by using a control projectile of know length and inserting it into the impact crater, the length of the projectile above the surface of the sample was then compared with the original length to determine the depth of the crater. The velocities for this test were determined using the calibration function for the micro-tester detailed in Chapter 3.

Table 4: Impact data for sea urchin spine cross sections

Sample	Velocity (m/s)	Impact Depth (mm)	Impact Energy (J)
1	*20*	*0.8890*	*7.222E-03*
2	*30*	*1.3208*	*1.625E-02*
3	*40*	*1.7780*	*2.889E-02*
4	*50*	*2.2098*	*4.514E-02*

The impact energy was calculated using a simple kinetic energy equation solved with the mass of the projectile and the respective projectile velocity before imapact.

$$KE = \frac{1}{2}mv^2 \tag{4.1}$$

The resulting data was then plotted to visualize the results as well as investigate trends over the various impacts (**Figure 30**). **Figure 30,i** shows that there is a linear relationship between the impact depth and the velocity of the projectile with an almost perfect correlation to the results. The following graph (**Figure 30,ii**) shows that there is a nearly square root relationship between the impact depth and the impact energy of the projectile with again a near perfect correlation between the two.

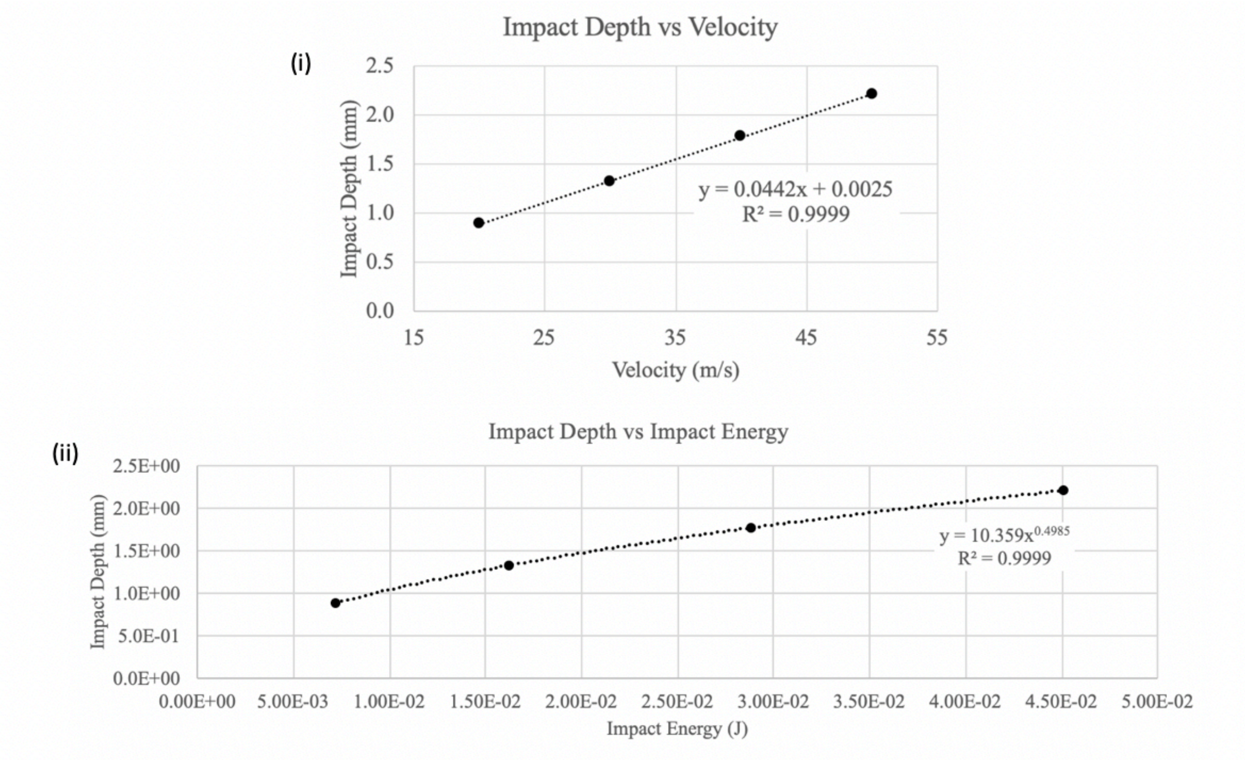

Figure 30: Plotted data of impact tests on sea urchin spine cross sections with respective trend lines. (i) Impact depth versus velocity. (iii) Impact depth versus impact energy.

The resulting impact craters were also subjected to micro computerized topography (μ-CT) scanning to characterize the respective compaction during the impact event. Individual slices of the sample were imaged and then compiled together to produce a three-dimensional scan of the sea urchin cross-section. Figure 24 shows the resulting scans of the impact sites. These scans were taken horizontally and then compiled using software to re-slice the stack of images in the vertical direction to show the penetration of the projectile into the sea urchin spine cross section. Of note is the elongated white region at the very bottom of the impact crater (**Figure 31**). This is the fractured and compacted region of the porous microstructure of the ceramic foam. In this context, it is known as the densified region as the material becomes physically denser in that area and provides a characterization of the crack propagation through the material at the bottom of the impact crater. The tabulated maximum depth of this region is shown in **Table 5** below.

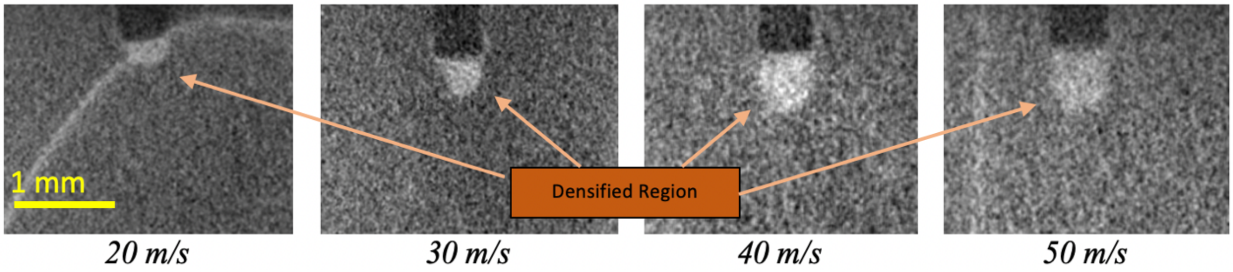

Figure 31: μ-CT scan images of bottom of impact site for the specified velocities. Image shows growing densified region in correlation to increased velocity.

Table 5: Densified region depth vs projectile impact velocity

Velocity (m/s)	*Densified Region Depth (mm)*
20	*0.2308*
30	*0.3654*
40	*0.5192*
50	*0.7308*

Graphing this data shows a linear trend between the densified region depth and the initial projectile velocity (**Figure 32**). The trend line shows an R^2 value of 0.9888 which suggests strong linear correlation between the depth of material compaction and velocity.

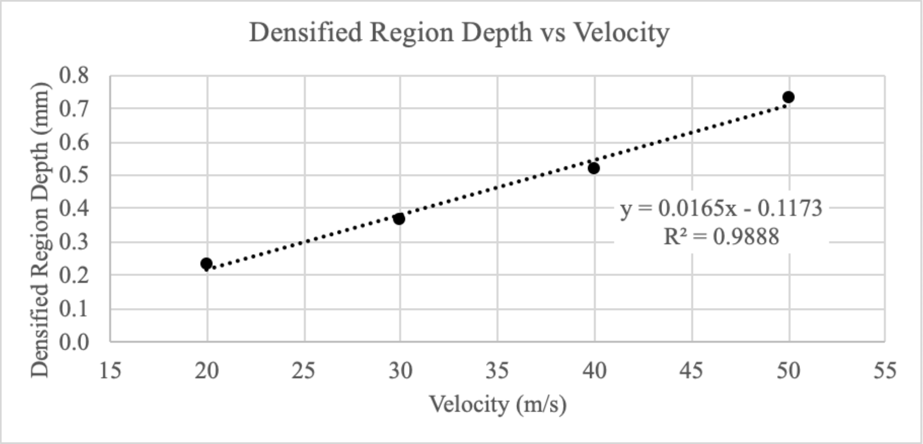

Figure 32: Plotted data for densified region of sea urchin spine as a function of projectile velocity

To analyze the impact absorption capabilities of the ceramic foam found in sea urchin spines, it was necessary to first characterize the mass normalized impact energy absorption of the material. The mass normalized impact energy absorption allows the ceramic foam to be compared to other materials' impact resistance on a micro and macro-scale. The total damaged depth of the impact site was calculated by adding together the depth of the impact crater and the densified region of the spine at the bottom of the impact location. The total damaged depth was then multiplied by the cross-sectional area of the projectile to determine the total damaged volume of the impact. The impact participation mass (permanently deformed target material) was computed by multiplying the damaged volume by the density of calcite (2709 kg/m^3) and the relative density of the calcite in the foam microstructure (10%) [34]. The impact energy of each test at the respective velocity was then divided by the impact participation mass to calculate the mass normalized impact energy absorption of the material (**Table 6)**. A graph of the normalized impact energy versus velocity is shown in **Figure 33** below. All of the projectiles for this test were stopped in the target samples themselves without rebounding, meaning that all of the impact energy was absorbed. If the projectile had rebounded after striking the sample or traveled completely through the sample, the absorbed energy from the impact would be calculated by comparing the initial kinetic energy of the projectile with the kinetic energy of the projectile after impact.

Table 6: Mass normalized impact energy absorption data for 20-50 m/s velocities

Velocity (m/s)	**Total Damaged Depth (mm)**	**Total Damaged Volume (mm^3)**	**Total Damaged Mass (kg)**	**Mass Normalized Impact Energy Absorption (MJ/kg)**
20	*1.120*	*0.220*	*5.956E-08*	*0.121*
30	*1.686*	*0.331*	*8.969E-08*	*0.181*
40	*2.297*	*0.451*	*1.222E-07*	*0.236*
50	*2.941*	*0.577*	*1.564E-07*	*0.289*

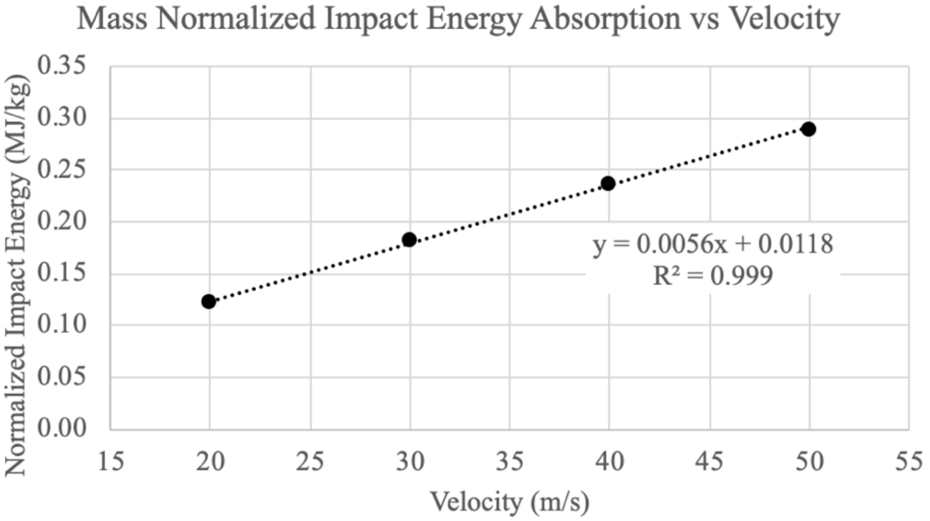

Figure 33: Plot of mass normalized impact energy absorption vs velocity

Included in **Figure 33** is a trendline of the normalized impact energy absorption versus the velocity of each test which shows a strong linear correlation between the two. The comparison of these values with those of other materials shows that the biological ceramic foam found in sea urchin spines is an extremely efficient impact resistant material by weight, especially at relatively low impact velocities [35]. For example, the architected porous calcite of the sea urchin spine outperforms aluminum, steel, and Kevlar in impact resistance when normalized by weight [35].

A sample volumetric reconstruction of one of the impacted sea urchin samples was also performed using the μ-CT scan data to provide a three-dimensional visualization of the impact location. A sample that was impacted with a projectile speed of 20 m/s was chosen for this reconstruction. An orthographic cross-sectional view of the impact crater is shown in **Figure 34** along with a top down view of the impact location shown in **Figure 35**. To create these solids, software was used to analyze the μ-CT image stack and turn the solid regions of the sample into binary information (1 for a solid region, 0 for a void). The individual slices were then analyzed to remove signal noise and a smoothing effect was applied to further clean up the binary data for the impacted region. The binary information was then compiled into a volumetric solid representation of the entire sample.

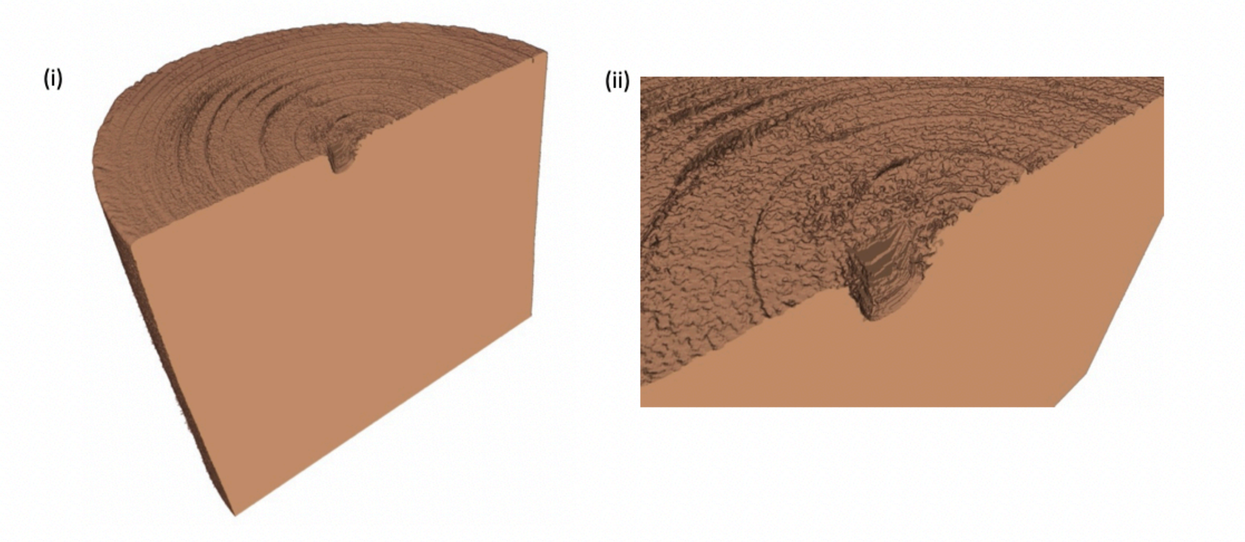

Figure 34: Orthographic cross-section view of sea urchin spine volumetric reconstruction. (i) Complete overview of impacted sample. (ii) zoomed in image of impact cross-section.

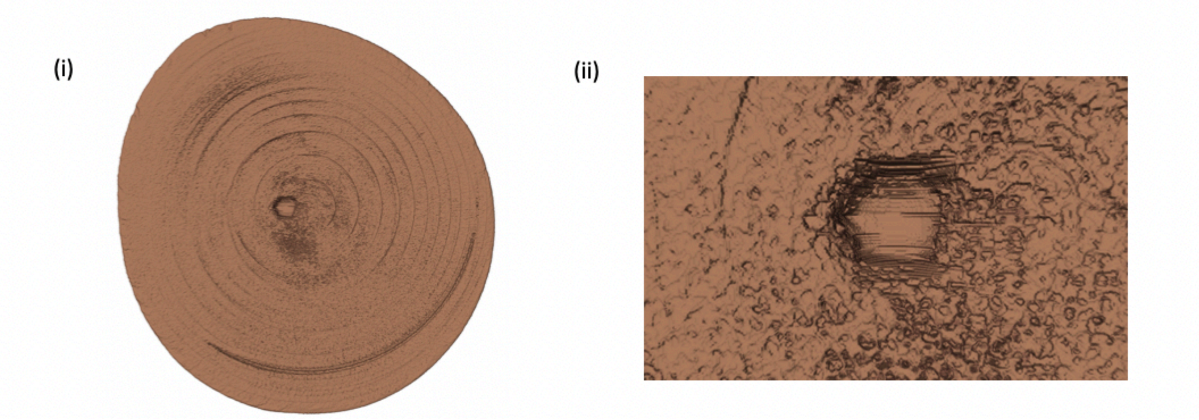

Figure 35: Top down view of impacted sea urchin volume reconstruction with (i) showing a complete sample view and (ii) showing a zoomed in image of the impact crater.

These impact reconstructions play an important role in the analysis of the impact as it provides a corroboration of the penetration depth of the projectile as well as a way to view the bottom of the impact sight without destroying the sample. A digital measurement of the impact depth was analyzed using image analysis software and compared with the analog measurement processes that relied on a control projectile and its height from the top reference surface of the sea urchin spine. These values were equal to each other for the sea urchin spine sample impact tests dictated in this thesis work which suggests that both methods of measurement are valid. Another important use of the volumetric reconstruction is it provides the shape of the impacted region, especially at the very bottom of the impact crater. Digital reconstruction provides a way to analyze and quantify the geometry of the bottom of the impact crater which is difficult to do with the real-life sample using non-destructive methods.

4.4 Radial Density Variation of Sea Urchin Spines

The internal microstructure of sea urchin spines is a functionally graded material with a changing density between the center radius of the spine and the outer edges which warrants a study of the impact properties along the radius of the samples. Studies show that the relative density of the center section of sea urchin spines is around 10% by volume which corresponds with a porosity of 90% whereas along the periphery of the spine the relative density is 45%, or 55% porosity [34]. An SEM image of a sea urchin spine cross section showing the radial variation in the relative density of the porous microstructure is presented in **Figure 36**. The image shows that the relative size of the branching of the ceramic foam is significantly smaller at the center section of the spine compared with that at the edge of the sample which corresponds to the decrease in density at the center of the sample.

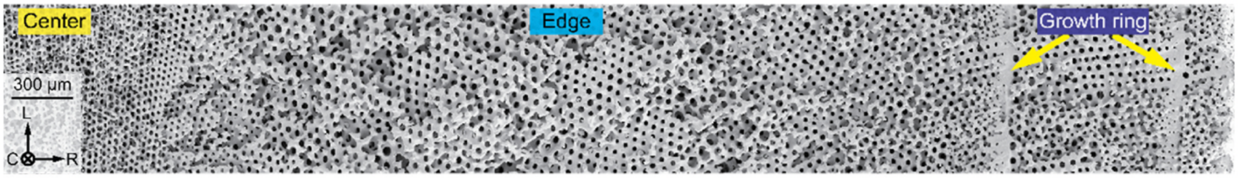

Figure 36: SEM image of sea urchin spine cross section showing radial variation of porous microstructure relative density. Adapted from [34]

To investigate how the change in relative density affects the impact properties of the material, a second set of spine samples were subjected to impact testing with a constant velocity of 40 m/s while the radial position of the impact was changed. Four samples were tested with three impact locations chosen along the radius of the cross section for two samples and two impact locations along the radius of the remaining two samples. The samples were then grouped together into two tests to have a total of five impact locations across the radius of the sea urchin spine. A schematic of the combined impact locations can be seen in **Figure 37**. This was done to provide adequate spacing between each impact location to mitigate the interference from the damaged microstructure around each impact site.

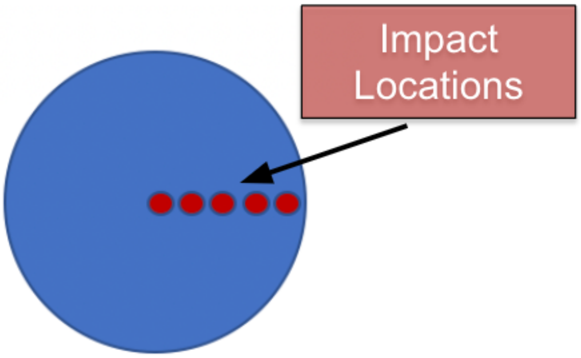

Figure 37: Schematic for impact locations along cross-section radius

The radius position of the sample was marked out as a percentage of the radius with the location varying between 0 to 80 % with a step over of 20 % between each location. The radial position was measured in percentage to account for the slight variation in overall diameter of the samples. The data for this test is tabulated in **Table 7**.

Table 7: Impact depth vs radial position data (40 m/s projectile speed)

Radial Position (%)	*Test 1 impact depth (mm)*	*Test 2 impact depth (mm)*	*Avg. Impact Depth (mm)*
0	*1.092*	*1.103*	*1.098*
20	*1.016*	*1.004*	*1.010*
40	*0.914*	*0.894*	*0.904*
60	*0.762*	*0.754*	*0.758*
80	*0.635*	*0.587*	*0.611*

The data for this test was then plotted to show the relationship between impact depth and radial position (**Figure 38**). As expected, the impact depth decreases as a function of radial position with the largest impact depth observed at the center of the cross section where the relative density is the lowest and the smallest impact depth occurring at the dense edge of the sample. The trendline shows a linear correlation between the radial location and the impact depth. Shown in **Figure 39** is an image of one of the tested samples as well as a μ-CT scan of the impact craters showing the depth of penetration into the sample as well as the densified region at the bottom of the crater. Further analysis using μ-CT scanning and image processing software is needed to precisely correlate the exact local relative density and penetration resistance to determine the mass normalized impact energy absorption of the sample at a specific position along the radius.

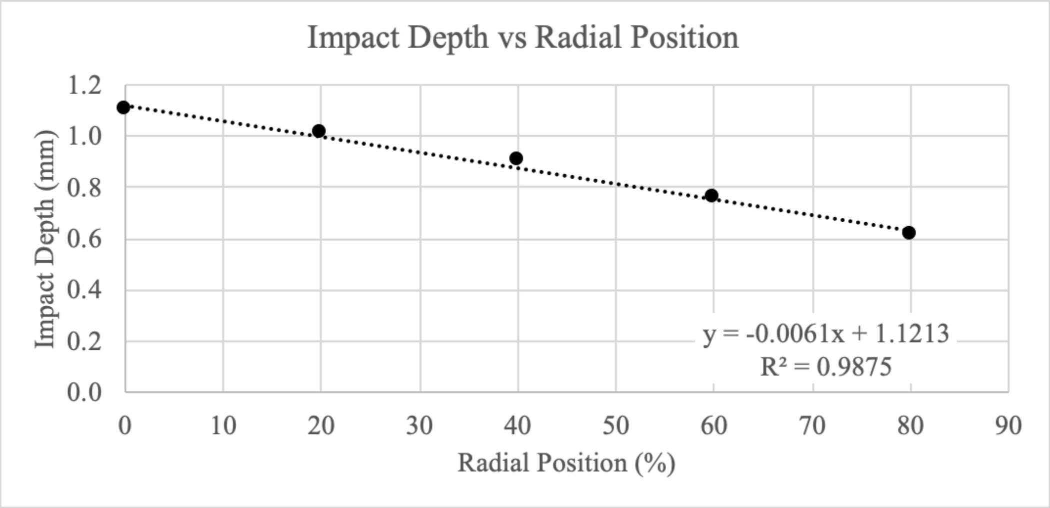

Figure 38: Graph of impact depth vs radial position with associated trendline

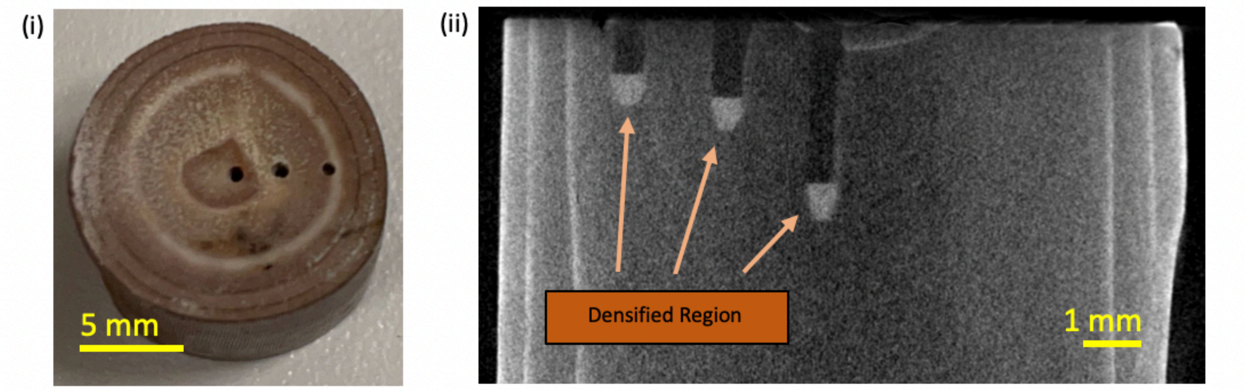

Figure 39: (i) Impacted test sample with varying radial position of impact. (ii) μ-CT scan of impacted sample showing depth of penetration and densified region.

4.5 Conclusions on Use of Impact Tester for Sea Urchin Spine Impact Properties

The results in this short study show that the micro impact tester is a viable option when wanting to investigate biological samples; in this case biological ceramic foams. The calculations and investigation shown above is only an example of the types of properties that can be investigated with the tester. Even with a small sample size, the tests show the important relationship between impact depth and impact energy for this particular material. These tests could easily be expanded upon to determine more about the impact absorbing properties of the ceramic foam structure of sea urchin spines. For example, if slow-motion video capture was utilized in conjunction with the test, the impulse that the projectile imparts on the sample could be calculated by determining the amount of time that the projectile takes to fully come to rest in the target sample. In addition, if a thinner sample of the sea urchin spine was utilized and the projectile fully passed through the sample, the impact absorption properties of the ceramic foam could be investigated by studying the velocity of the projectile before and after impacting the sample. This would also allow for the study of the fracture mechanics of the sea urchin spine microstructure by studying the fracture patterns of the material during impact. Finally, scanning election microscopy (SEM) and transmission electron microscopy (TEM) could be used to study the physical microstructure of the calcite that makes up the spines and study them before and after impact to determine the specific crack propagation through the material upon impact. As stated, there are many ways that the micro-impact tester could be utilized to expand upon the current research into sea urchin spine material properties with the tests shown as part of this thesis acting as an example of what is possible with this scale of tester. The micro-impact tester is already scheduled to be utilized in the lab for further research of sea urchin spines to investigate some of the impact properties outlined above and to model a system for bio-inspired impact resistant ceramic foams; proving the device's validity when small-scale impact testing is needed.

Chapter 5

Future Use Cases

The micro impact tester was not intended to only be used for sea urchin spine impact property testing, but was designed with future experimental use cases in mind. There are numerous situations where a projectile impact tester of this size and velocity range would be useful in determining material properties in response to impact loading events, especially in biological and bio-inspired material applications. Such future planned use cases of the impact tester include a comprehensive study of mantis shrimp dactyl clubs in response to high speed dynamic loading as well as a cross department study of particulate impacts on axial gas turbine engine airfoil blades.

5.1 Mantis Shrimp Dactyl Club

Mantis shrimp use their feeding appendages, known as dactyl clubs, to smash shells and impale fish at high rates of speed and tremendous forces in relation to their size [36]. The outer layers of these dactyl clubs are formed through a biomineralization process where calcium phosphate and chitin are layered together to form a naturally impact resistant material [37]. Extensive research has been performed on these dactyl clubs at low impact velocities to formulate inspired materials that replicate the intricate impact region and the periodic region of the dactyl club and the synergy that exists between the two. The interface and interaction between these two regions are what allows the dactyl club to have better impact resistance in comparison to other naturally occurring materials and this structuring and interface is what is being replicated to create bio-inspired impact resistant materials. [38]. However, to date, there has been very little research into the high-speed impact performance of these architected materials [39]. The speeds of mantis shrimp dactyl clubs have been observed to be on average 23 m/s with an impact force in excess of 1500 N, ideal conditions to be simulated using the small-scale impact tester [19]. There is current work going on in Virginia Tech's Biological and Bio-Inspired Materials Lab that would benefit greatly from the use of this thesis's micro projectile impact tester.

5.2 Axial Gas Turbine Engine Airfoil Particle Impact Research

Another area of research that has been theorized to benefit from the small-scale impact tester is the study of particle impacts on axial gas turbine engine blades. Gas turbine engines are constantly subjected to impacts from small projectiles and particulates during normal operation and different coatings and materials are being developed and tested for erosion performance [40]. Erosion effects are a serious problem for turbines operating in a particulate environment as they cause efficiency degradation and premature failure of components [41]. There is currently no impact tester at Virginia Tech that can perform these types of experiments and there have already been inter-department talks to utilize both the macro-scale and micro-scale projectile impact testers that have been developed as part of this thesis. The hope is to use both impact testers to research and develop better turbine blade coatings and materials as well as to gain a better understanding of their performance during adverse environmental conditions.

Chapter 6

Summary and Future Work

6.1 Summary

This thesis encompasses the design and fabrication of both a large-scale projectile impact tester as a proof of concept design as well as a micro-scale version that carries over many of the design elements of the large version but is designed to fire projectiles for small scale biological material tests. Also included as part of this thesis is a breakdown of the various impact testers currently available within research to show why this project was necessary.

The project culminated in simple impact studies of sea urchin spines to showcase the capabilities of the impact tester in its current form as well as to outline some of the expanded properties that could be determined with simple experimental setup changes. From this impact study, it was determined that sea urchin spines are a leading candidate in the formulation of bio-inspired impact resistant ceramic foams as they have excellent energy absorption properties during dynamic loading. The calcite foam structure of the sea urchin spines proved to have better impact absorption capabilities in comparison to many current engineering materials used for impact resistance. The final part of this thesis is a brief overview of the planned future use cases of the device. A detailed list of the main contributions from this thesis work is presented below:

- Conducted detailed literature review on current micro-impact testers utilized in research applications.
- Designed and built a large-scale impact tester as a proof of concept design, validated design equations and velocity calibration of device.
- Designed and built a micro-scale impact tester optimized for biological and bio-inspired samples, validated the velocity calibration as well as precision and accuracy of the device.
- Conducted impact study on sea urchin spine samples to investigate energy absorption capabilities and show the validity of micro-impact tester within biological sample testing.
- Presented planned future use cases of the impact testers and how the usability of the devices can be expanded upon.

6.2 Recommendations for Future Work

The intent of this thesis was to build and design a micro-projectile impact testing device for Virginia Tech’s Biological and Bio-Inspired Materials Lab with the intent of using it for future experiments for many different research topics and various use cases. Therefore, the capabilities of the tester are not limited to its current configuration and there are many areas that can be changed to facilitate different needs. Outlined below are changes that can be implemented in the future to expand the use of the micro-scale impact tester.

6.2.1 Projectile Profile and Use of Sabot

An area of future work that was not investigated as part of this thesis is the shape of the projectile tip as it is highly specific to the experiment being performed. By controlling the tip profile of the projectile, an experimenter can influence its penetration properties. For example, a pointed tip would penetrate deeper and easier than the flat blunt tip used during the experiments as part of this thesis work. A rounded dome shape could also be used to influence the fracture patterns seen in the target sample. Along this same line is the use of a sabot to fire a projectile smaller and lighter than the designed 0.5 mm projectile. As described earlier, a sabot is a carrier for the projectile that allows a smaller diameter projectile to still fit in the barrel and be used for experiments. The use of a sabot would also allow for particles to be fired from the tester to study impacts on the 10s of microns scale.

6.2.2 Barrel Length Change for Increased Velocity

Another consideration for future work to the tester is if greater velocities than the 50 m/s the device was designed for needed to be achieved for specific experiments. From the governing velocity equation created in Chapter 2 of this thesis, it can be seen that the final velocity of the projectile is directly tied to the length of the barrel. By increasing barrel length, the final velocity of the projectile will also increase. Therefore, it would be a simple matter to extend the velocity range of the device to increase its capabilities if needed.

6.2.3 In-Situ X-Ray Imagining

The end goal of the micro-scale impact tester is to incorporate the system into an in-situ x-ray diffraction imaging system, specifically the system at the Argonne National Lab. In-situ x-ray diffraction would allow for research into the 3D morphology and microstructure deformation of a sample during impact loading [42]. One thing that needs to be taken into consideration for this type of experimental setup is that the x-ray machine would need to be triggered precisely at the right time for imaging. To this end, the microcontroller that is integrated into the firing mechanism of the small-scale tester is already setup to send a timing signal to any piece of equipment that it is integrated into, making it a simple matter to program the correct timer based off of the chosen projectile velocity.

References

[1] D. Veysset, J.-H. Lee, M. Hassani, S. E. Kooi, E. L. Thomas, and K. A. Nelson, “High-velocity micro-projectile impact testing,” Applied Physics Reviews, vol. 8, no. 1, p. 011319, 2021.

[2] Z. P. Bažant, “Scaling laws in mechanics of Failure,” Journal of Engineering Mechanics, vol. 119, no. 9, pp. 1828–1844, 1993.

[3] Y.-T. Cheng and C.-M. Cheng, “Scaling, dimensional analysis, and indentation measurements,” Materials Science and Engineering: R: Reports, vol. 44, no. 4-5, pp. 91–149, 2004.

[4] R. J. Clifton, “Response of materials under dynamic loading,” International Journal of Solids and Structures, vol. 37, no. 1-2, pp. 105–113, 2000.

[5] J. E. Field, S. M. Walley, W. G. Proud, H. T. Goldrein, and C. R. Siviour, “Review of experimental techniques for high rate deformation and shock studies,” International Journal of Impact Engineering, vol. 30, no. 7, pp. 725–775, 2004.

[6] C. Rahner, H. A. Al-Qureshi, D. Stainer, D. Hotza, and M. C. Fredel, “Numerical Evaluation of a light-gas gun facility for impact test,” Modelling and Simulation in Engineering, vol. 2014, pp. 1–6, 2014.

[7] A. J. Stilp, “Sabot designs for launching penetrators and projectiles,” High-Pressure Shock Compression of Solids VIII, pp. 201–225.

[8] M. J. Burchell, M. J. Cole, J. A. McDonnell, and J. C. Zarnecki, “Hypervelocity impact studies using the 2 MV van de graaff accelerator and two-stage light gas gun of the University of Kent at Canterbury,” Measurement Science and Technology, vol. 10, no. 1, pp. 41–50, 1999.

[9] D. J. Grosch and J. P. Riegel, “Development and optimization of a ‘micro’ two-stage light-gas gun,” International Journal of Impact Engineering, vol. 14, no. 1-4, pp. 315–324, 1993.

[10] T. D. Aslam, M. A. McBride, N. Rai, D. E. Hooks, J. A. Stull, and B. J. Jensen, “Modeling atomically mixed graded density impactors,” Journal of Applied Physics, vol. 131, no. 22, p. 225901, 2022.

[11] L. C. Chhabildas, L. N. Kmetyk, W. D. Reinhart, and C. A. Hall, “Enhanced hypervelocity launcher - capabilities to 16 km/s,” International Journal of Impact Engineering, vol. 17, no. 1-3, pp. 183–194, 1995.

[12] T. J. Mitchell, M. A. F. Kendall, and B. J. Bellhouse, “A ballistic study of micro-particle penetration to the oral mucosa,” International Journal of Impact Engineering, vol. 28, no. 6, pp. 581–599, 2003.

[13] M. A. F. Kendall, “The delivery of particulate vaccines and drugs to human skin with a practical, hand-held shock tube-based system,” Shock Waves, vol. 12, no. 1, pp. 23–30, 2002.

[14] D. Rinberg, C. Simonnet, and A. Groisman, “Pneumatic capillary gun for ballistic delivery of microparticles,” Applied Physics Letters, vol. 87, no. 1, p. 014103, 2005.

[15] S. Yin, M. Meyer, W. Li, H. Liao, and R. Lupoi, “Gas flow, particle acceleration, and heat transfer in cold spray: A Review,” Journal of Thermal Spray Technology, vol. 25, no. 5, pp. 874–896, 2016.

[16] D. L. Paisley, S.-N. Luo, S. R. Greenfield, and A. C. Koskelo, “Laser-launched Flyer Plate and confined laser ablation for shock wave loading: Validation and Applications,” Review of Scientific Instruments, vol. 79, no. 2, p. 023902, 2008.

[17] A. D. Curtis, A. A. Banishev, W. L. Shaw, and D. D. Dlott, “Laser-driven flyer plates for shock compression science: Launch and target impact probed by Photon Doppler velocimetry,” Review of Scientific Instruments, vol. 85, no. 4, p. 043908, 2014.

[18] Z. P. Gu, Y. J. Cheng, K. L. Xiao, K. Li, X. Q. Wu, Q. M. Li, and C. G. Huang, “Geometrical scaling law for laser-induced micro-projectile impact testing,” International Journal of Mechanical Sciences, vol. 223, p. 107289, 2022.

[19] W. Huang, M. Shishehbor, N. Guarín-Zapata, N. D. Kirchhofer, J. Li, L. Cruz, T. Wang, S. Bhowmick, D. Stauffer, P. Manimunda, K. N. Bozhilov, R. Caldwell, P. Zavattieri, and D. Kisailus, “A natural impact-resistant bicontinuous composite nanoparticle coating,” Nature Materials, vol. 19, no. 11, pp. 1236–1243, 2020.

[20] E. A. Eid, M. M. Sadawy, and A. M. Reda, “Computing the dynamic friction coefficient and evaluation of radiation shielding performance for AISI 304 Stainless Steel,” Materials Chemistry and Physics, vol. 277, p. 125446, 2022.

[21] S.-B. Li and J.-X. Xie, “Fabrication of thin-walled 316L stainless steel seamless pipes by extrusion technology,” Journal of Materials Processing Technology, vol. 183, no. 1, pp. 57–61, 2007.

[22] E. B. Zaretsky, “Light Gas Gun,” in Hypervelocity launchers, SPRINGER, 2018, pp. 3–19.

[23] F. H. Kim, D. Penumadu, N. Kardjilov, and I. Manke, “High-resolution X-ray and neutron computed tomography of partially saturated granular materials subjected to projectile penetration,” International Journal of Impact Engineering, vol. 89, pp. 72–82, 2016.

[24] Z. Ruirui and G. Xiao, “The application and development of Photoelectric Sensor,” Energy Procedia, vol. 17, pp. 1304–1308, 2012.

[25] “Photoelectric sensors,” OMRON. [Online]. Available: https://www.ia.omron.com/support/guide/43/introduction.html. [Accessed: 09-Apr-2023].

[26] D. Poobathy and R. M. Chezian, “Edge detection operators: Peak Signal to noise ratio based comparison,” International Journal of Image, Graphics and Signal Processing, vol. 6, no. 10, pp. 55–61, 2014.

[27] J. Koupil and V. Vícha, “Simple phenomena, slow motion, surprising physics,” Physics Education, vol. 46, no. 4, pp. 454–460, 2011.

[28] “Kron Technologies.” [Online]. Available: https://www.krontech.ca/wp-content/uploads/2021/09/RE-PDEV-10009-Chronos-User-Manual-Full-Software-Version-0.7.0.pdf. [Accessed: 10-Apr-2023].

[29] M. Tomin and Á. Kmetty, “Polymer foams as advanced energy absorbing materials for sports applications—a review,” Journal of Applied Polymer Science, vol. 139, no. 9, p. 51714, 2021.

[30] F. Yin, B. Nie, Y. Wei, S. Lin, and X. Wang, “Explosion suppression effect and mechanism analysis of ceramic foam in the horizontal pipe,” Energy Sources, Part A: Recovery, Utilization, and Environmental Effects, vol. 44, no. 3, pp. 7176–7193, 2022.

[31] A. A. Lakis, A. Oulmane, and L. E. Iliescu, “Satellites/Spacecraft Materials and Hypervelocity Impact (HVI) Testing: Numerical Simulations,” European Journal of Mechanical Engineering Research, vol. 3, no. 3, pp. 41–77, Aug. 2016.

[32] N. Tsafnat, J. D. Fitz Gerald, H. N. Le, and Z. H. Stachurski, “Micromechanics of sea urchin spines,” PLoS ONE, vol. 7, no. 9, 2012.

[33] T. Yang, Z. Jia, Z. Wu, H. Chen, Z. Deng, L. Chen, Y. Zhu, and L. Li, “High strength and damage-tolerance in echinoderm stereom as a natural bicontinuous ceramic cellular solid,” Nature Communications, vol. 13, no. 1, 2022.

[34] H. Chen, T. Yang, Z. Wu, Z. Deng, Y. Zhu, and L. Li, “Quantitative 3D structural analysis of the cellular microstructure of sea urchin spines (ii): Large-volume structural analysis,” Acta Biomaterialia, vol. 107, pp. 218–231, 2020.

[35] C. M. Portela, B. W. Edwards, D. Veysset, Y. Sun, K. A. Nelson, D. M. Kochmann, and J. R. Greer, “Supersonic impact resilience of nanoarchitected carbon,” Nature Materials, vol. 20, no. 11, pp. 1491–1497, 2021.

[36] S. N. Patek, W. L. Korff, and R. L. Caldwell, “Deadly strike mechanism of a mantis shrimp,” Nature, vol. 428, no. 6985, pp. 819–820, 2004.

[37] S. Amini, M. Tadayon, J. J. Loke, A. Kumar, D. Kanagavel, H. Le Ferrand, M. Duchamp, M. Raida, R. M. Sobota, L. Chen, S. Hoon, and A. Miserez, “A diecast mineralization process forms the tough mantis shrimp dactyl club,” Proceedings of the National Academy of Sciences, vol. 116, no. 18, pp. 8685–8692, 2019.

[38] Q. Han, S. Shi, Z. Liu, Z. Han, S. Niu, J. Zhang, H. Qin, Y. Sun, and J. Wang, “Study on impact resistance behaviors of a novel composite laminate with basalt fiber for helical-sinusoidal bionic structure of Dactyl Club of mantis shrimp,” Composites Part B: Engineering, vol. 191, p. 107976, 2020.

[39] R. P. Behera and H. Le Ferrand, “Impact-resistant materials inspired by the mantis shrimp's Dactyl Club,” Matter, vol. 4, no. 9, pp. 2831–2849, 2021.

[40] W. Tabakoff and M. Metwally, “Coating effect on particle trajectories and turbine blade erosion,” Journal of Engineering for Gas Turbines and Power, vol. 114, no. 2, pp. 250–257, 1992.

[41] B. Taherkhani, A. P. Anaraki, J. Kadkhodapour, N. K. Farahani, and H. Tu, “Erosion due to solid particle impact on the turbine blade: Experiment and simulation,” Journal of Failure Analysis and Prevention, vol. 19, no. 6, pp. 1739–1744, 2019.

[42] K. J. Gross, S. Guthrie, S. Takara, and G. Thomas, “In-situ X-ray diffraction study of the decomposition of NaAlH4,” Journal of Alloys and Compounds, vol. 297, no. 1-2, pp. 270–281, 2000.